Influence of clay colloids, humic acid and water chemistry on the stability, aggregation and deposition of nanoscale titanium dioxide ($nTiO_2$)

by

© Zhong Tang

A Thesis submitted to the

School of Graduate Studies

in partial fulfillment of the requirements for the degree of

Master of Science

Department of Earth Sciences

Memorial University of Newfoundland

December 2017

St. John's Newfoundland

ABSTRACT

Fate and transport of engineered nanoscale titanium dioxide ($nTiO_2$) have received much attention during the past decade. The stability, concurrent aggregation and deposition of $nTiO_2$ in water with complicated components, however, have not been fully examined. The objective of this thesis was to determine the individual and synergistic effect of pH, cation valence, humic acid, Fe/Al oxyhydroxide coatings and clay colloids on $nTiO_2$ stability, aggregation and deposition, and elucidate the related mechanisms. We conducted systematic laboratory experiments to determine $nTiO_2$ stability, aggregation and deposition onto a quartz sand in NaCl and $MgCl_2$ solutions, both in the absence and presence of humic acid and clay colloids. Results showed that $nTiO_2$ formed hetero-aggregates and the hetero-aggregates may either deposit or remain suspended depending on their interactions with quartz sand and Fe/Al oxyhydroxide coatings. Humic acid was found to make $nTiO_2$ stable to prevent $nTiO_2$ aggregation and deposition under most conditions.

ACKNOWLEDGEMENTS

I would like to express my gratitude to my supervisor, Dr. Tao Cheng, for offering mentorship all the time during my research. He dedicates himself to research and teaching, and his professional ethics inspired me a lot. The help he offered in both studying and life made my two-year graduate life wonderful.

My appreciation also goes to Dr. Penny Morril for serving on my Master committee and valuable advices on my research.

Special thanks are given to Dr. Valerie Booth for the use of zetasizer, Inês Nobre Silva for the digestion and ICP-MS measurements, Wanda Aylward for the XRD and SEM measurements and Pam King for her help with grinding and sieving quartz sand.

Besides, I gratefully acknowledge financial support from the Natural Sciences and Engineering Research Council of Canada (NSERC) Discovery Grant and School of Graduate Studies Fellowship provided by Memorial University of Newfoundland.

The last but not least, I need to thank all lab colleagues for their too many helps during the two years.

Table of Contents

List of Tables

List of Figures

List of abbreviations and symbols

°C – Degree Celsius

cm – centimeter

EDL– electrical double layer

EDX– energy dispersive X-ray

g – gram

HA – humic acid

h^{-1} – per hour

IS – ionic strength

J – joule

$k_B T$– energy unit equals 4.11×10^{-21} J

kg – kilogram

L – liter

mL/min – milliliter per minute

M – mole

mM – millimole

mg – milligram

ml – milliliter

mg/kg – milligrams per kilogram

mg/L –milligrams per liter

mm – millimeter

mol/L – moles per liter

mV – millivolts

nm – nanometer

NOM – natural organic matter

pH – power of hydrogen; a measure of hydrogen ion activity

PZC – point of zero charge

SEM – scanning electron microscope

µg – microgram

µg/L – micrograms per liter

µm – micrometer

VDW – van der Waals

XRD – X-ray diffraction

List of Appendices

Chapter 1: Introduction and Overview

1.1 Environmental risks of engineered titanium dioxide nanoparticle

Titanium dioxide nanoparticles ($nTiO_2$), one of the most extensively used nanoscale materials, have been universally utilized in products, including sunscreens (Gondikas et al., 2014), paints (Al-Kattan et al., 2014), coatings (Santos et al., 2014), photocatalysts (Morales-Torres et al., 2012) and environmental catalysts (Tada et al., 2014). The increasing use of $nTiO_2$ in industrial and household application will inevitably lead to the release of such materials into the environment, which poses a potential threat to the environment (Coll et al., 2015). When $nTiO_2$ enters natural aquatic systems, it could cause contamination issues to the water resource. It has been revealed that $nTiO_2$ could facilitate the transport of some pollutants such as Cu in natural aquatic systems (Fang et al., 2011). The toxicity of $nTiO_2$ to aquatic organisms and microorganisms has been elucidated by some studies showing that $nTiO_2$ could either enter the cells or be in intimate contact with the cell walls to cause toxicity (Aruoja et al., 2009; Heinlaan et al., 2008). Moreover, environmental factors such as humic acid (HA) and ionic strength (IS) are very influential to the toxicity of $nTiO_2$ in aquatic environment according to a study illustrating that the HA and IS both could protect aquatic organisms from oxidative stress of $nTiO_2$ (Fang et al., 2015). Studying the fate of $nTiO_2$ in subsurface systems is essential for evaluating the environmental risks of $nTiO_2$.

1.2 Aggregation and deposition of $nTiO_2$ in aquatic environments

When $nTiO_2$ is released into aquatic systems, the stability and mobility of $nTiO_2$ govern its fate in aquatic systems (Nawack and Bucheli, 2007). Some water chemistries (pH, IS etc.) and co-existence nanoparticles could boost particle - particle or particle - surface interactions which lead to aggregations or depositions onto collectors, while some water chemistries and co-existence nanoparticles could enhance $nTiO_2$ stability (Fatisson et al., 2009; Thio et al., 2011). Natural water physicochemical characteristics such as ions, pH, temperature, IS all have important impact on interactions among simultaneously existing nanoparticles and collectors (Zhao et al., 2012; Gallego-Urrea et al., 2014). When water pH is lower than the point of zero charge (PZC) of $nTiO_2$, $nTiO_2$ carries positive surface charge and the surface charge density (and therefore the stability of the suspended $nTiO_2$ particles) increases when pH decreases. When pH is higher than the PZC, $nTiO_2$ has negative surface charge and the surface charge density (and therefore the stability of the suspended $nTiO_2$ particles) increases when pH increases (Loosli et al., 2015). When pH values are close to PZC, the surface charge of $nTiO_2$ is low and the van der Waals attraction overcomes the repulsive electrostatic force, resulting in $nTiO_2$ agglomeration (French et al., 2009). IS is another important factor that impacts the behaviour of $nTiO_2$ in aquatic systems. It was demonstrated that the magnitude of surface charge decreased with an increase in IS either in monovalent or divalent ion electrolytes, due to the electrostatic double layer compression (Chen et al., 2011). When IS increases, the compression effects on the electrostatic double layer become stronger, and at high IS, the repulsive force between nanoparticles reduces to the degree where $nTiO_2$ aggregates (Solovitch et al., 2010).

Clay particles, such as kaolinite, montmorillonite, illite, and chlorite, are the most abundant inorganic colloids in aquatic systems (Wilson et al., 2014), and they could strongly influence the fate of engineered nanoparticles in aquatic system (Cai et al., 2014). Zhou et al. (2012) found that the impact of montmorillonite on $nTiO_2$ stability is pH dependent. At pH 4, montmorillonite reduced the stability of $nTiO_2$ nanoparticles because the positively charged $nTiO_2$ particles bridged the negatively charged montmorillonite particles through electrostatic attraction. While at pH 8, montmorillonite did not influence the stability of $nTiO_2$ since both montmorillonite and $nTiO_2$ were negatively charged.

Natural organic matter (NOM) is ubiquitous in nature (Nebbioso and Piccolo, 2013) and plays a critical role in the stability and mobility of colloidal particles and nanoparticles (Aiken et al., 2011). Humic acid is the main component of NOM and it has been observed that the presence of HA normally enhanced the stability and transport of $nTiO_2$ via electrostatic and steric effects (Chen et al., 2012; Erhayem and Sohn., 2014; Jung et al., 2014; Liu et al., 2010; Liu et al., 2011; Wang et al., 2013). The presence of HA has influence on $nTiO_2$, clay and sand grains interactions. HA was an important component of natural organic matter (NOM) and has strong ability to modify $nTiO_2$ surface characteristics by attaching onto $nTiO_2$ surface, therefore influencing $nTiO_2$ aggregation and deposition (Thio et al., 2011).

1.3 Thesis objectives

Although much progress has been made to understand the behaviors of $nTiO_2$ in aquatic environment, stability, and concurrent aggregation and deposition of $nTiO_2$ in natural water, especially in water with complicated components, have not been fully

examined. Moreover, mechanisms of particle stability, aggregation and deposition in the presence of divalent cations and co-existing clay colloids and NOM need to be elucidated. Systematic laboratory experiments were conducted to determine $nTiO_2$ stability, aggregation and deposition in NaCl and $MgCl_2$ solutions, both in the absence and presence of HA and clay colloids. Zeta potential (ZP) and hydrodynamic diameter (HDD) were measured to obtain information on electrical charges and particle aggregation. Furthermore, interaction energy profiles were calculated to provide theoretical explanation and insight into the experimental results.

The objectives of this study were to better understand (1) the individual and synergistic effect of cation valence, HA, and illite colloids on $nTiO_2$ stability and aggregation, and ascertain the mechanisms involved in $nTiO_2$ aggregation and stability in the presence of multiple components; (2) the influence of pH, HA, and Fe/Al oxyhydroxide coatings on concurrent aggregation and deposition of $nTiO_2$ in the presence of clay colloids

1.4 Co-authorship statement

I am the author of this thesis. The first manuscript (Chapter 2) was co-authored with my supervisor, Dr. Tao Cheng, and the second manuscript (Chapter 3) was co-authored with Dr. Tao Cheng and Leanne M. Fisher-Power. I am the 1st author for both manuscripts and I am the principal author for this thesis including the MSc research proposal, experimental design, experiments implementation, data collection and analysis, and manuscript composition. All research work above was conducted under the guidance of my supervisor. I characterized the quartz sand with the assistance from Wanda Aylward (SEM-EDX). I set up the laboratory experiment systems for batch experiments and performed the

batch experiments. I prepared the samples for ICP-MS analysis with the assistance from Inês Nobre Silva. I measured the zeta potential and particle size of all the $nTiO_2$ and clay colloid suspensions. Leanne M. Fisher-Power measured the zeta potential of quartz sand. I processed all the raw data, analyzed the data with the guidance from my supervisor and composed the manuscripts.

1.5 Reference

Aiken, G. R., Hsu-Kim, H., Ryan, J. N. (2011) Influence of dissolved organic matter on the environmental fate of metals, nanoparticles, and colloids. *Environ. Sci. Technol*. 45, 3196−3201.

Al-Kattan, A., Wichser, A., Zuin, S., Arroyo, Y., Golanski, L., Ulrich, A., Nowack, B. (2014) Behavior of TiO_2 Released from Nano-TiO_2-Containing Paint and Comparison to Pristine Nano-TiO2. *Environ. Sci. Technol*. 48, 6710-6718.

Aruoja, V., Dubourguier, H., Kasemets, K., Kahru, A. (2009) Toxicity of nanoparticles of CuO, ZnO and TiO_2 to microalgae Pseudokirchneriella subcapitata. *Science of the Total Environment* 407, 1461–1468.

Cai, L.; Tong, M.; Wang, X.; Kim, H. (2014) Influence of clay particles on the transport and retention of titanium dioxide nanoparticles in quartz sand. *Environ. Sci. Technol*. 48, 7323-7332.

Chen, G., Liu, X., Su, C. (2011) Transport and Retention of TiO_2 Rutile Nanoparticles in Saturated Porous Media under Low-Ionic-Strength Conditions: Measurements and Mechanisms. *Langmuir* 27, 5393–5402.

Chen, G.; Liu, X.; Su, C. (2012) Distinct effects of humic acid on transport and retention of TiO_2 Rutile Nanoparticles in saturated sand columns. *Environ. Sci. Technol*. 46, 7142-7150.

Coll, C., Notter, D., Gottschalk, F., Sun, T., Som, C., Nowack, B. (2015) Probabilistic environmental risk assessment of five nanomaterials (nano-TiO_2, nano-Ag, nano-ZnO, CNT, and fullerenes). *Nanotoxicology* 1743-5404.

Erhayem. M., Sohn, M. (2014) Stability studies for titanium dioxide nanoparticles upon adsorption of suwannee river humic and fulvic acids and natural organic matter. *Science of the Total Environment* 468-469, 249-257.

Fang, J., Shan,X. Q., Wen, B., Lin, J. M., Owens, G., Zhou, S. R. (2011) Transport of copper as affected by titanium nanoparticles in soil columns. *Environmental Pollution* 159, 1248-1256.

Fang, T., Yu, L. P., Zhang, W. C., Bao, S. P. (2015) Effects of humic acid and ionic strength on TiO_2 nanoparticles sublethal toxicity to zebrafish. *Ecotoxicology* 24, 2054–2066.

Fatisson, J., Domingos, F. R., Wilkinson, J. K., and Tufenkji, N. (2009) Deposition of TiO_2 nanoparticles onto silica measured using a quartz crystal microbalance with dissipation monitoring. *Langmuir* 25 (11), 6062–6069.

French, R. A., Jacobson, A. R., Kim, B., Isley, S. L., Penn, R. L., Baveye, P. C. (2009) Influence of ionic strength, pH, and cation valence on aggregation kinetics of titanium dioxide nanoparticles. *Environ. Sci. Technol*. 43, 1354–1359.

Gallego-Urrea, A. J., Holmberg, P. J., and Hassellöv, M. (2014) Influence of different types of natural organic matter on titania nanoparticle stability: effects of counter ion concentration and pH. *Environ. Sci. Nano*. 1, 181–189.

Gondikas, A. P., Kammer, F., Reed, R. B., Wagner, S., Ranville, J. F., Hofmann, T. (2014) Release of TiO_2 Nanoparticles from Sunscreens into Surface Waters: A One-Year Survey at the Old Danube Recreational Lake. *Environ. Sci. Technol*. 48, 5415-5422.

Heinlaan, M., Ivask, A., Blinova, I., Dubourguier, H., & Kahru, A. (2008) Toxicity of nanosized and bulk ZnO, CuO and TiO_2 to bacteria Vibrio fischeri and crustaceans Daphnia magna and Thamnocephalus platyurus. *Chemosphere* 71, 1308–1316.

Jung, B., O'Carroll, D., Sleep, B. (2014) The influence of humic acid and clay content on the transport of polymer-coated iron nanoparticles through sand. *Science of the Total Environment* 496, 155-164.

Liu, X., Wazne, M., Han, Y., Christodoulatos, C., Jasinkiewicz, K. L. (2010) Effects of natural organic matter on aggregation kinetics of boron nanoparticles in monovalent and divalent electrolytes. *Journal of Colloid and Interface Science* 348, 101–107.

Liu, X., Wazne, m., Chou, T., Xiao, R., Xu, S. (2011) Influence of Ca^{2+} and Suwannee River Humic Acid on aggregation of silicon nanoparticles in aqueous media. Water Research 45, 105-112.

Loosli, F., Coustumer, P. L., Stoll, S. (2015) Effect of electrolyte valency, alginate concentration and pH on engineered TiO_2 nanoparticle stability in aqueous solution. *Science of the Total Environment* 535, 28–34.

Morales-Torres, S., Pastrana-Martínez, L. M., Figueiredo, J. L., Faria, J. L., Silva, A. M. T. (2012) Design of graphene-based TiO_2 photocatalysts—a review. *Environ Sci Pollut Res.* 19, 3676–3687.

Nebbioso, A., Piccolo, A. (2013) Molecular characterization of dissolved organic matter (DOM): a critical review. *Anal Bioanal Chem*. 405, 109–124.

Nowack, B., Bucheli, T.D. (2007). Occurrence, behavior and effects of nanoparticles in the environment. Environmental Pollution 150, 5–22.

Santos, A., Araujo, J. R., Landi, S. M., Kuznetsov, A., Granjeiro, J. M., Sena, L. A´., Achete, C. A. (2014) A study of the physical, chemical and biological properties of TiO_2 coatings produced by micro-arc oxidation in a Ca–P-based electrolyte. *J Mater Sci: Mater Med*. 25,1769–1780.

Solovitch, N., Labille, J., Rose, J., Chaurand, P., Chneck, D., Wiesner, M. R., Bottero, J. (2010) Concurrent aggregation and deposition of TiO_2 nanoparticles in a sandy porous media. *Environ. Sci. Technol*. 44, 4897–4902

Tada, H., Jin, Q., Iwaszuk, A., Nolan, M. (2014) Molecular-Scale Transition Metal Oxide Nanocluster SurfaceModified Titanium Dioxide as Solar-Activated Environmental Catalysts. *J. Phys. Chem. C*. 118, 12077−12086.

Thio, B. J. R., Zhou, D., Keller, A. A. (2011) Influence of natural organic matter on the aggregation and deposition of titanium dioxide nanoparticles. *Journal of Hazardous Materials*. 189, 556–563.

Wang, D., Zhang, W., Zhou, D. (2013) Antagonistic effects of humic acid and iron oxyhydroxide grain-coating on biochar nanoparticle transport in saturated sand. *Environ. Sci. Technol*. 47, 5154-5161.

Wilson, M. J., Wilson, L., Patey, I. (2014) The influence of individual clay minerals on formation damage of reservoir sandstones: a critical review with some new insights. *Clay Miner.* 49, 147–164.

Zhao, Y., Gu, X., Gao, S., Geng, J., Wang, X. (2012) Adsorption of tetracycline (TC) onto montmorillonite: Cations and humic acid effects. *Geoderma* 183–184, 12–18.

Zhou, D., Abdel-Fattah, A. I., & Keller, A. A. (2012) Clay Particles Destabilize Engineered Nanoparticles in Aqueous Environments. *Environ. Sci. Technol*. 46, 7520−7526.

Chapter 2: Stability and aggregation of nanoscale titanium dioxide particle ($nTiO_2$): Effect of cation valence, humic acid, and clay colloids

Abstract

Fate and transport of engineered nanoscale titanium dioxide ($nTiO_2$) have received much attention during the past decade. The aggregation and stability of $nTiO_2$ in water with complicated components, however, have not been fully examined. The objective of this study was to determine the individual and synergistic effects of cation valence, humic acid, and clay colloids on $nTiO_2$ stability and aggregation, and elucidate the related mechanisms. Systematic laboratory experiments were conducted to determine $nTiO_2$ stability and aggregation in NaCl and $MgCl_2$ solutions, both in the absence and presence of humic acid and illite colloids. Results showed that Mg^{2+}, in comparison to Na^+, could make the zeta potential of $nTiO_2$ more positive, and shift the point of zero charge of $nTiO_2$ ($pH_{pzc,TiO2}$) towards higher pH. $nTiO_2$ were destabilized by illite colloids at pH < $pH_{pzc,TiO2}$ through formation of illite-$nTiO_2$ hetero-aggregates, but were not interfered by illite colloids at higher pH. HA was found to make $nTiO_2$ stable via electrostatic and steric effects, both in the absence and presence of illite colloids. Calculated interaction energy based on Derjaguin-Landau-Verwey-Overbeek (DLVO) theory revealed that instability of the $nTiO_2$ suspensions was mainly caused by primary minima, and that secondary minima normally do not destabilize the suspension, even though they are found to promote aggregation.

Keywords: nanoscale titanium dioxide ($nTiO_2$); divalent cation; humic acid (HA); illite colloid; zeta potential; hydrodynamic diameter; DLVO interaction energy

2.1 Introduction

Nanoscale titanium dioxide ($nTiO_2$) materials have been synthesized and introduced into the environment due to the production, usage, and disposal of $nTiO_2$ containing products (Boncagin et al., 2009; Al-Kattan et al., 2014; Gondikas et al., 2014). Although addition of $nTiO_2$ to some materials enhances the quality and performance of the product, many studies have shown that $nTiO_2$ could be toxic to aquatic microorganisms and organisms, and may cause environmental problems (Aruoja et al., 2008; Heinlaan et al., 2008; Coll et al., 2015). Similar to naturally-occurring submicron-sized particulate matters like clay colloids, $nTiO_2$ was found to adsorb solute contaminants such as heavy metals and may influence their movement in groundwater (Fang et al., 2011). Therefore, fate and transport of $nTiO_2$ has been an interesting research topic due to its relevance to water quality and contaminant transport in subsurface environment.

$nTiO_2$ particles are mobile in soil and groundwater when they remain suspended in water and not attach to the immobile soil and sediment grains. To stay suspended, $nTiO_2$ particles must be small enough, so that they are not susceptible to gravity sedimentation. Besides, repulsive forces between particles must be high enough so that the particles do not attract to each other to form large aggregates. Aggregation not only influences particle stability but also particle transport in aquatic systems (Nowack et al., 2007; Chowdhury et al., 2011). Interactive forces between particles, which govern the aggregation and stability of $nTiO_2$, are controlled largely by the electrical charge of the particle, and affected by water chemical conditions such as pH, ionic strength (IS), and ion composition (Dosmingos et al., 2009; French et al., 2009; Erhayem and Sohn et al., 2014; Gallego-Urrea et al., 2014).

$nTiO_2$ particle develops its electrical charges via protonation/deprotonation of surface functional groups, and adsorption of charged ions to the electrical double layer (Ludwig and Schindler, 1995). Surface charge of $nTiO_2$, and therefore its aggregation and stability, are pH dependent and influenced by co-existing cations and anions. Substantial increase in $nTiO_2$ size was found when pH approaching the point of zero charge (PZC) of $nTiO_2$ (i.e., the pH at which the surface is neutral and carries no net charges) (Loosli et al., 2013; Wu and Cheng, 2016), and $nTiO_2$ aggregation was observed in water with higher IS due to the greater compression of the electrical double layer, which reduced repulsive forces (Chen et al., 2011).

Aggregation and stability of $nTiO_2$ in natural water are complicated by the presence of divalent cations (e.g., Ca^{2+} and Mg^{2+}), dissolved organic matter (DOM), and clay colloids. Many studies showed that natural DOM adsorbed to colloid and nanoparticle surface and enhanced the stability of the particle via electrostatic and steric effects (Liu et al., 2010, 2011; Aiken et al., 2011; Chen et al., 2012; Nebbioso and Piccolo, 2013; Wang et al., 2013; Erhayem and Sohn., 2014; Jung et al., 2014). Wu and Cheng (2016), however, observed that humic acid (HA), an important type of NOM, may promote aggregation and destabilize $nTiO_2$ by neutralizing surface charges. It was found that divalent cations could promote aggregation and destabilize $nTiO_2$ by adsorbing to the particle (Loosli et al. 2015). Divalent cations were also found to increase DOM adsorption to $nTiO_2$ via bridging effect, in which the cation connected carboxylic group of DOM with surface sites on $nTiO_2$ (Liu et al., 2010, 2011; Erhayem and Sohn, 2014). Zhang et al. (2009) reported that Ca^{2+} could destabilize NOM-coated nanoparticles via bridging effect.

Clay colloids, the most abundant inorganic particles in aquatic systems (Wilson et al., 2014), may interact with and influence the aggregation and stability of co-existing particles (Jiang et al., 2010; Zhou et al., 2012; Amirianshoja et al., 2013; Wang et al., 2015). The nature of the interaction between clay particle and other particles depends on water chemistry and property of the particles. Clay colloids and $nTiO_2$ could have different PZC, hence, within in certain pH range, clay colloids and $nTiO_2$ may carry opposite charges, leading to hetero-aggregation (i.e., formation of clay-$nTiO_2$ aggregates). Zhou et al. (2012) found that the impact of montmorillonite on $nTiO_2$ stability is pH dependent, since surface charges of the particles changed with pH. Cai et al. (2014) showed that clay particles may either facilitate, hinder, or not influence the stability and mobility of engineered nanoparticles depending on pH, IS, and type and properties of the clay particle. Divalent cations were reported to promote hetero-aggregation between clay particle and engineered nanoparticle through bridging effect (Torkzaban et al., 2012).

Although much progress has been made to understand the behaviors of $nTiO_2$ in aquatic environment, aggregation and stability of $nTiO_2$ in natural water, especially in water with complicated components, have not been fully examined. For example, divalent cation, DOM, and clay colloids often co-exist, however, very few studies investigated their combined effects (e.g., Lee et al., 2016). Moreover, mechanisms of particle aggregation and stability in the presence of divalent cations and co-existing colloids and DOM need to be elucidated. The objective of this study was to determine the individual and synergistic effect of cation valence, HA, and illite colloids on $nTiO_2$ stability and aggregation, and ascertain the mechanisms involved in $nTiO_2$ aggregation and stability in the presence of

multiple components. Systematic laboratory experiments were conducted to determine $nTiO_2$ stability in NaCl and $MgCl_2$ solutions, both in the absence and presence of HA and illite colloids. Zeta potential (ZP) and hydrodynamic diameter (HDD) were measured to obtain direct information on electrical charges and particle aggregation. Furthermore, interaction energy profiles were calculated to provide theoretical explanation and insight into the experimental results.

2.2 Materials and Methods

2.2.1 Preparation of materials

All the chemicals were certified ACS grade and purchased from VWR International Co. Nanopure water, with resistivity >18.2 MΩ-cm and dissolved organic carbon (DOC) concentration < 0.02 mg/L, was used for preparation of all the solutions and particle suspensions.

Nanoscale titanium dioxide ($nTiO_2$) powder (Aeroxide™ TiO_2 P25) with > 99.5% purity (Fisher Scientific) was used to prepare $nTiO_2$ particle suspensions. The specific surface area of the powder is 35−65 m^2/g according to the manufacturer, and X-ray diffraction (XRD) analysis showed that the powder is a mixture of anatase (90%) and rutile (10%) with primary particle size of 23 and 40 nm respectively (Wu and Cheng, 2016).

$nTiO_2$ particle suspension. $nTiO_2$ powder was weighed using an analytical balance and suspended in background solution to achieve the desired $nTiO_2$ concentration. The $nTiO_2$ suspension was then sonicated using a Branson Digital Sonifier (Crystal Electronics) for 30 min with 120 W power to disperse the particles and get a homogeneous suspension.

HA stock solution. 100 mg HA powder (Alfa Aesar) was dissolved in 100 mL nanopure water to achieve a HA concentration of 1000 mg/L. The HA stock solution was stored in darkness at 4 ℃ in a fridge for all our experiments.

Illite colloid stock suspension. 4 g illite powder (IMt-2 Illite-Cambrianshale, The Clay Mineral Society) was mixed with 1000 mL nanopure water and sonicated using a Branson Digital Sonifier for 30 min with 120 W power to disperse the illite particles. The mixture was then let stand for 24 hours to remove large particles before the supernatant from the mixture was carefully transferred into a high-density polyethylene (HDPE) bottle for storage. Illite colloid stock thus prepared was used in subsequent experiments for preparation of particle suspensions. To determine illite concentration of the illite colloid stock, 100 mL stock suspension was filtered through a 0.1 μm polyethersulfone membrane filter (Pall Life Sciences) and the filter was oven dried at 60 ℃. The weight difference before and after the filtration divided by the volume (100 mL) equaled illite concentration. The procedure was performed in triplicate and the mean value was taken as the illite concentration of the stock suspension.

2.2.2 Stability test

To investigate how clay colloids and HA interact with and influence the stability of $nTiO_2$ particles, five types of particle suspension ($nTiO_2$, illite, $nTiO_2$+illite, $nTiO_2$+HA, and $nTiO_2$+HA+illite) were prepared, and their stability in 4 types of background solutions (i.e., 1 mM NaCl, 10 mM NaCl, 0.5 mM $MgCl_2$ and 1 mM $MgCl_2$) at different pH (5, 7, and 9) was examined (Table 1).

Table 1. $nTiO_2$, illite, and humic acid (HA) concentrations in the suspensions for the stability tests

Suspension type*	Components	$nTiO_2$ concentration (mg/L)	Illite concentration (mg/L)	HA concentration (mg/L)
1	$nTiO_2$	50	-	-
2	Illite	-	10	-
3	$nTiO_2$ + illite	50	10	-
4	$nTiO_2$ + HA	50	-	10
5	$nTiO_2$ + illite +HA	50	10	10

*Each type of suspension was prepared in four types of background solution (i.e., 1 mM NaCl, 10 mM NaCl, 0.5 mM $MgCl_2$, and 1 mM $MgCl_2$), and for each type of background solution, three pH (i.e., 5, 7 and 9) were tested.

$nTiO_2$ suspensions were prepared following the procedure described in Section 2.2.1, and illite colloid suspensions were made by diluting the illite colloid stock suspension. $nTiO_2$+illite, $nTiO_2$+HA, and $nTiO_2$+HA+illite suspensions were prepared by mixing $nTiO_2$, illite, and HA suspensions/solutions at appropriate ratios. When preparing the $nTiO_2$+HA+illite suspensions, $nTiO_2$ and HA were well mixed before illite stock suspension was added. To adjust IS of the sample, NaCl or $MgCl_2$ powder was weighted using an analytical balance and added to the suspensions. After IS adjustment, the samples were sonicated for 30 min with 120 W power in order to mix and disperse the particles. pH of the suspensions was adjusted using small volumes of 0.1 M NaOH and/or HCl solutions.

Once prepared, light absorbance of the suspensions was measured using an UV-Vis spectrophotometer (Genesys 10S UV-Vis, Thermo Scientific) to determine the initial absorbance (A_0). Then the suspensions were tightly capped and let stand on the bench. Every 30 minutes, supernatant from each suspension was taken for light absorbance (A) measurement until the last sample was taken at t = 360 minutes. All the tests were performed in duplicate.

To maximize sensitivity, a wavelength of 280 nm was used for measuring light absorbance of the illite suspensions (Suspension Type 2, Table 1). A wavelength of 600 nm was used for measuring light absorbance of the pure and mixed $nTiO_2$ suspensions (i.e., Suspension Type 1, 3, 4, and 5, Table 1). Cai et al. (2014) showed that at a wavelength of 600 nm, absorbance of clay particle suspensions and HA was low, but absorbance was sensitive to suspended $nTiO_2$ concentration. Our preliminary tests confirmed that by using a wavelength of 600 nm, light absorbance of the illite colloid suspension and HA was negligible, while light absorbance of $nTiO_2$ was still substantial (Figure A1).

2.2.3 Zeta potential (ZP) and hydrodynamic diameter (HDD) measurement

Samples for ZP and HDD measurement were prepared using the same procedures as those used for the stability tests. ZP and HDD of the suspensions were measured using a Zetasizer (Zetasizer Nano ZS, Malvern) two hours after the samples were being prepared, which allowed aggregation to occur in unstable suspensions. All the ZP and HDD measurements were performed in triplicate.

2.2.4 Calculation of the interactive energy between particles

Derjaguin-Landau-Verwey-Overbeek (DLVO) theory (Van Olphen, 1963) was employed to study the interactions between particles. By assuming sphere–sphere geometry, Equation (1) and (2) were used to calculate the London-van der Waals (LW) force and electric double layer (EDL) force between two particles (Gregory, 1981, Chen et al., 2011). The overall DLVO force is the sum of the LW and EDL forces. Although the assumption of sphere geometry is not perfect for layer clays such as illite colloids, it enables us to make approximate estimations of the DLVO energy.

$$\emptyset_{LW} = -\frac{AR_1R_2}{6D(R_1+R_2)}\left[1-\frac{5.32D}{\lambda}\ln\left(1+\frac{\lambda}{5.32D}\right)\right]^{-1} \quad (1)$$

$$\emptyset_{EDL} = \frac{2\pi R_1R_2n_\infty k_BT}{(R_1+R_2)\kappa^2}\left(\psi_c{}^2+\psi_s{}^2\right)\left\{\frac{2\psi_c\psi_s}{\psi_c{}^2+\psi_s{}^2}\ln\left[\frac{1+\exp(-\kappa D)}{1-\exp(-\kappa D)}\right]+\ln[1-\exp(-2\kappa D)]\right\} \quad (2)$$

where A (J) is Hamaker constant, R (m) is particle radius, D (m) is separation distance, λ is the characteristic wavelength of interaction (10^{-7} m), n_∞ is number concentration of the bulk ion, κ (m^{-1}) is the Debye–Hückel reciprocal length, and $\kappa = 2.32\times10^9\ (\Sigma C_iZ_i^2)^{1/2}$, where C_i is the concentration of ion i and Z_i is the valency value. ψ_c (V) and ψ_S (V) are surface potential of the particles. In our calculation zeta potential was used to approximate surface potential.

In the $nTiO_2$+illite systems, the ZP and HDD measured by a zetasizer reflected the overall properties of the mixed particles and therefore ZP and HDD of the individual particle were not known. Under these circumstances, ZP and HDD were measured in the individual system (i.e., $nTiO_2$ and illite system) to approximate the properties of $nTiO_2$ and illite in the mixed systems. Similarly, in the $nTiO_2$+illite+HA systems, ZP and HDD were taken from the individual measured results (i.e., results from the $nTiO_2$+HA systems, and the illite systems). HA is known to adsorb to $nTiO_2$ particle and influence the ZP and HDD of the particle. However, HA adsorption to illite particles is negligibly low since both illite and HA are negatively charged. A number of studies have shown low adsorption of humic substances to clay minerals (e.g., Rashid et al., 1972; Dumat and Staunton, 1999). As a result, we assumed that HA adsorption and its influence on the ZP and HDD of $nTiO_2$ particles in the $nTiO_2$+illite+HA systems were similar to those in the $nTiO_2$+HA systems.

The Hamaker constant (A) of the $nTiO_2$-water-$nTiO_2$ system is 3.5×10^{-20} J (Gómez-Merino et al., 2007), and is 2.2×10^{-20} J for the illite-water-illite system (Long et al., 2006).

The Hamaker constant of the $nTiO_2$-water-illite system is calculated as 3.6×10^{-20} J, using Equation (3) (Hiemenz, 1997).

$$A_{132} = (\sqrt{A_{11}} - \sqrt{A_{33}})(\sqrt{A_{22}} - \sqrt{A_{33}}) \quad (3)$$

where 1 is $nTiO_2$, 2 is illite, and 3 is water, and the following constants: $A_{TiO2\text{-}TiO2}$ = 1.53×10^{-19} J (Bergström, 1997), $A_{H2O\text{-}H2O} = 3.7\times10^{-20}$ J (Israelachvili, 2011), and $A_{illite\text{-}illite}$ = 1.4×10^{-19} J (Novich & Ring, 1984).

2.3 Results and Discussion

2.3.1 $nTiO_2$ stability

In 1 mM NaCl and 10 mM NaCl solutions, the relative absorbance (A/A_0) of the $nTiO_2$ particle suspension was stable ($A/A_0 \approx 1$)at pH 5 and 9 up to 360 minutes, but decreased from 1.0 to 0.37 at pH 7 (Figure 1a and 1b), indicating that the suspension was stable at pH 5 and 9, but unstable at pH 7.

At pH 5 and 9, the stability was due to the repulsive electrostatic forces between $nTiO_2$ particles. $nTiO_2$ particles were positively charged at pH 5, with zeta potential of 24.5 to 30.7 mV (Figure 2a). While at pH 9, $nTiO_2$ particles were negatively charged with zeta potential of -34.1 to -38.9 mV (Figure 2a). The charges at these pH resulted in high energy

Table 2. The pH, Zeta Potential (ZP), and Hydrodynamic Diameter (HDD) of the suspensions in NaCl solutions, and the Energy Barrier ($\emptyset_{max}$), Secondary Minimum ($\emptyset_{2min}$) Calculated for the particle-particle interaction based on DLVO theory. *N/A means not applicable.

Suspension	NaCl (mM)	pH	ZP (mV)	HDD (nm)	Hamaker Constant (* 10^{-20} J)	Energy Barrier (k_BT)	Secondary Minimum (k_BT)
$nTiO_2$	1	5	24.5	269.0	3.5	29.7	-0.1
		7	-2.8	3033.7	3.5	N/A	N/A*
		9	-38.9	522.6	3.5	193.0	-0.1
	10	5	30.7	779.1	3.5	115.7	-3.7
		7	-2.1	6779.7	3.5	N/A	N/A
		9	-34.1	661.4	3.5	175.6	-2.9
illite	1	5	-24.4	324.0	2.2	41.7	-0.1
		7	-27.6	355.4	2.2	62.6	-0.1
		9	-29.4	311.7	2.2	64.4	-0.1
	10	5	-29.3	630.3	2.2	129.1	-1.7
		7	-29.4	483.8	2.2	99.9	-1.3
		9	-29.9	327.6	2.2	70.6	-0.8
$nTiO_2$ + illite	1	5	17.6	2351.3	3.6	N/A	N/A
		7	0.2	5550.0	3.6	1.3	-0.4
		9	-34.6	419.0	3.6	221.8	-0.1
	10	5	16.6	6607.7	3.6	N/A	N/A
		7	-6.0	4808.3	3.6	N/A	N/A
		9	-36.1	1258.7	3.6	270.3	-1.9
$nTiO_2$ + HA	1	5	-38.6	254.0	3.5	92.2	-0.1
		7	-39.3	255.9	3.5	97.0	-0.1
		9	-38.9	250.2	3.5	92.5	-0.1
	10	5	-38.0	655.7	3.5	228.7	-2.7
		7	-39.0	833.1	3.5	309.9	-3.3
		9	-42.4	718.8	3.5	326.7	-0.2
$nTiO_2$ + HA + illite	1	5	-36.7	268.1	3.6	85.8	-0.1
		7	-39.0	264.9	3.6	98.6	-0.1
		9	-39.6	246.1	3.6	95.0	-0.1
	10	5	-39.2	663.8	3.6	238.5	-2.5
		7	-44.4	692.2	3.6	350.3	-2.6
		9	-43.7	508.3	3.6	247.8	-1.9

barrier between particles. The calculated energy barrier were 29.7 k_BT (pH 5) and 193.0 k_BT (pH 9) respectively in 1 mM NaCl solution, and 115.7 k_BT (pH 5) and 175.6 k_BT (pH 9) respectively in 10 mM NaCl solution (Table 2). The high energy barrier prevented the particles from aggregating and kept the suspensions stable.

At pH 7, ZP of $nTiO_2$ was near neutral (i.e., -2.8 and -2.1 mV respectively in 1 mM and 10 mM NaCl solution) (Figure 2a), therefore the electrostatic repulsive force was weak, and the calculated DLVO energy profile showed no energy barrier (Table 2), indicating particle aggregation and unstable suspension.

In $MgCl_2$ solutions, $nTiO_2$ was stable at pH 5 but unstable at pH 7 and 9 (Figure 1c, 1d). ZP measurements showed that ZP of $nTiO_2$ in $MgCl_2$ solutions were similar to those in NaCl solutions at pH 5, but very different from those in NaCl solutions at pH 7 and 9. At pH 7 and 9, ZP of $nTiO_2$ in $MgCl_2$ solution were mostly positive (Figure 2f), as opposed to the negative ZP in NaCl solutions (Figure 2a). Unlike monovalent ions such as Na^+, which influenced ZP mainly through screening effect, divalent ions such as Mg^{2+} adsorbed to the surface sites on $nTiO_2$ and changed the ZP of $nTiO_2$ particles from negative to positive (Loosli et al., 2015). Ludwig and Schindler (1995) showed that protonation/deprotonation of surface hydroxyl groups controls the surface charge of $nTiO_2$, and divalent cations can adsorb to TiO_2 via formation of surface complexes with hydroxyl groups. Our ZP measurement results showed that Mg^{2+} adsorption was strong at pH 7 and 9, due to the attractive electrostatic forces between $nTiO_2$ and Mg^{2+}. At pH 5, however, adsorption was weak, since $nTiO_2$ carried positive charge and repelled the like-charged Mg^{2+}.

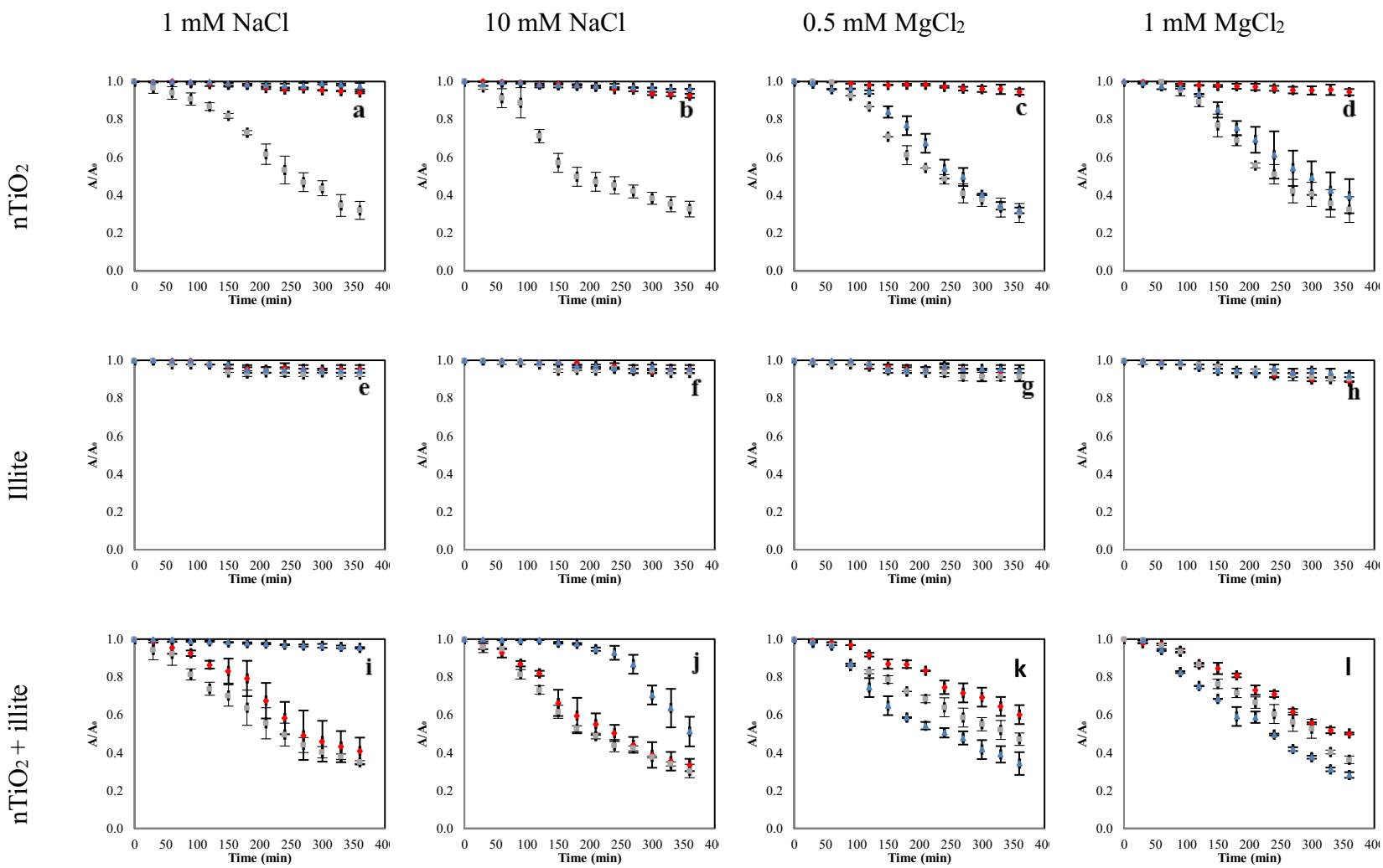
1 mM NaCl
10 mM NaCl
0.5 mM MgCl2
1 mM MgCl2
nTiO2
Illite
nTiO2 + illite
A/A0
Time (min)
a
b
c
d
e
f
g
h
i
j
k
l

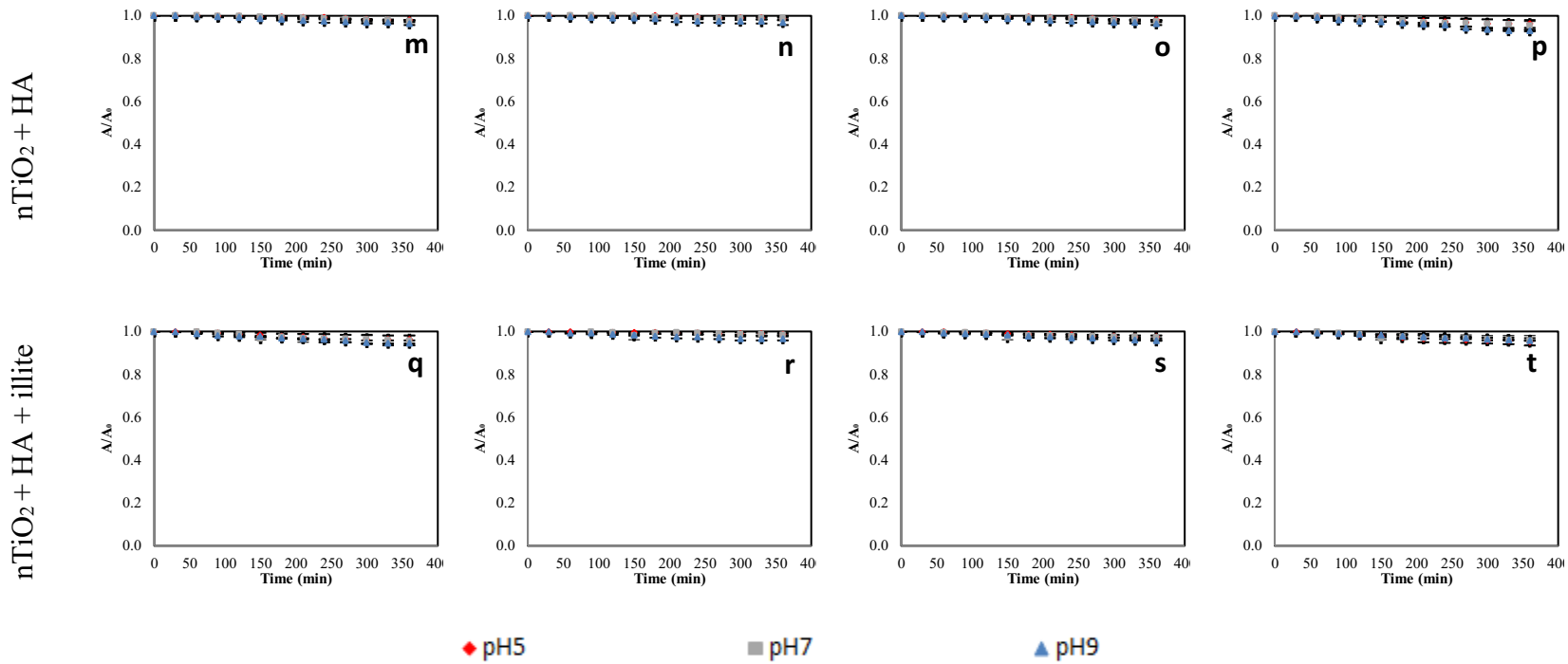

Figure 1. Stability of the suspensions at pH 5, 7, and 9 in 1 mM NaCl (a, e, i, m, q), 10 mM NaCl (b, f, j n, r), 0.5 mM $MgCl_2$ (c, g, k, o, s), and 1 mM $MgCl_2$ (d, h, l, p, t) solutions. Data is expressed as mean ± standard deviation of duplicate experiment.

At pH 5, ZP of $nTiO_2$ was around +30 mV in $MgCl_2$ solutions (Figure 2f), and the stability of the suspension was caused by the repulsive electrostatic forces between $nTiO_2$ particles. DLVO calculation results confirmed the presence of high energy barriers at pH (40.6 k_BT and 75.0 k_BT in 0.5 and 1 mM $MgCl_2$, respectively) (Table 3). At pH 7 and 9, net charges on $nTiO_2$ were low (ZP < 15 mV), and DLVO calculation results showed no energy barriers between particles in either 0.5 or 1 mM $MgCl_2$ solutions (Table 3), indicating unstable suspensions, in agreement with the stability test results.

2.3.2 Illite particle stability

In NaCl solutions, illite was stable throughout the whole duration of the experiment for all the pH and IS (Figure 1e, 1f). It was also found that IS and pH had minimum influence on the ZP of illite under the tested conditions (Figure 2b), i.e., the ZP were -24.4 mV, -27.6 mV and -29.4 mV respectively at pH 5, 7, and 9 in 1 mM NaCl solution, and -29.3 mV, -29.4 mV and -29.9 mV respectively in 10 mM NaCl solution. DLVO calculation results showed that the energy barrier between illite particles were high (> 41 k_BT), indicating stable suspension (Table 2).

In $MgCl_2$ solutions, illite was also stable for all the pH and IS tested (Figure 1g, 1h). Unlike $nTiO_2$, which became positively charged in 1 mM $MgCl_2$ solutions, illite particles were negatively charged in the $MgCl_2$ solutions, with ZP ranging from -12 to -17 mV (Figure 2g), less negative than those in NaCl solutions (~ -30mV) (Figure 2b). While metal oxides such as $nTiO_2$ adsorb metal ions via specific surface sites, clay minerals like illite adsorb via cation exchange process, and the binding strength of clay minerals for metal ions is usually weaker than that of metal oxides (Bradl, 2004; Alessi et al., 2010). The

negative ZP of illite vs. the positve ZP of $nTiO_2$ in the $MgCl_2$ solutions under our experimental conditions indicated lower Mg^{2+} adsorption capacity of illite relative to that of $nTiO_2$. The less negative ZP of illite in $MgCl_2$ solutions vs. those in NaCl solutions was attributable to the stronger adsorption and sreeening effect of Mg^{2+} in comparison to Na^+.

The HDD of illite in $MgCl_2$ solutions were larger than those in NaCl solutions (Figure 3g vs. 3b), which was atributable to the lower repulsive forces in $MgCl_2$ solutions, and potentially the "bridging effect". Divalent cations were reported to promote aggregation by connecting clay particles via cation exchange sites (Torkzaban et al., 2012). DLVO calculation showed that energy barriers between illite particles for all pH in $MgCl_2$ solutions are lower compared to those in NaCl solution, but high enough (>25 k_BT) to sustain stable suspensions (Table 3), consistent with the stability test results.

2.3.3 $nTiO_2$ stability with co-existing illite particles

In NaCl solutions, when illite was present, $nTiO_2$ was unstable at pH 5 and 7 (Figure 1i, 1j). At pH 5 in 1 mM and 10 mM NaCl solutions, illite was negatively charged (-24.4 mV and -27.6 mV), but $nTiO_2$ was positively charged (24.5 mV and 30.7 mV), therefore no energy barrier existed between $nTiO_2$ and illite particles, resulting in aggregation. At pH 7, $nTiO_2$ was unstable by itself (Figure 1a and 1b), and adding illite did not prevent aggregation, as indicated by the close-to-neutral ZP of the $nTiO_2$+illite mixture (i.e., 0.2 mV and -6.0 mV respectively in 1 mM and 10 mM NaCl solution) (Figure 2c). The calculated DLVO profiles showed either no energy barrier or low energy barrier (1.3 k_BT) at pH 5 and 7, consistent with the stability test results.

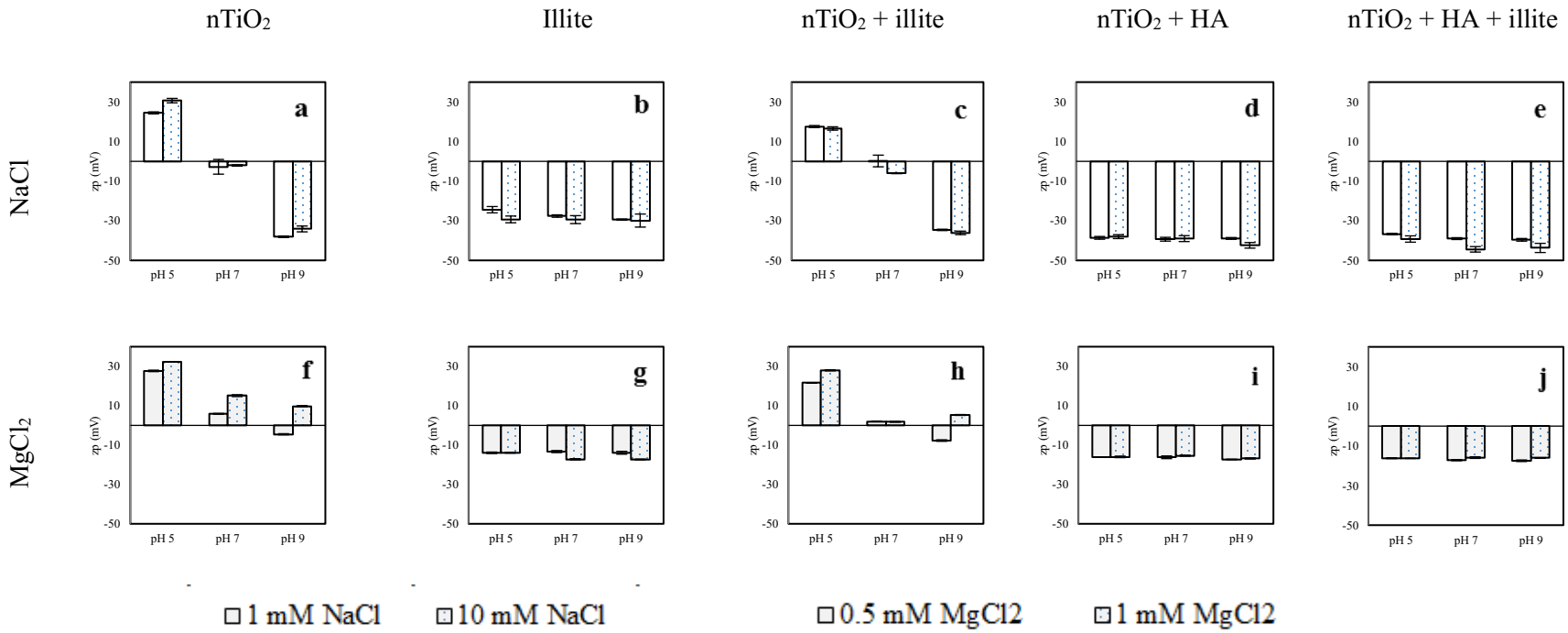

Figure 2. Zeta potential (ZP) of the suspensions at pH 5, 7, and 9 in 1 mM NaCl (blank), 10 mM NaCl (spotted), 0.5 mM $MgCl_2$ (grey), and 1 mM $MgCl_2$ (grey spotted) solutions. Data is expressed as mean ± standard deviation of triplicate measurement.

Table 3. The pH, Zeta Potential (ZP), and Hydrodynamic Diameter (HDD) of the suspensions in $MgCl_2$ solutions, and the Energy Barrier ($\emptyset_{max}$) and Secondary Minimum ($\emptyset_{2min}$) calculated for the particle-particle interaction based on DLVO theory

Suspension	$MgCl_2$ (mM)	pH	ZP (mV)	HDD (nm)	A (* 10^{-20} J)	$\emptyset_{\max}$ (k_BT)	$\emptyset_{2\min}$ (k_BT)
$nTiO_2$	0.5	5	27.7	275.7	3.5	40.6	-0.2
		7	5.9	6099.0	3.5	N/A	N/A
		9	-4.5	6973.7	3.5	N/A	N/A
	1.0	5	32.4	323.8	3.5	75.0	-0.4
		7	15.1	7217.7	3.5	N/A	N/A
		9	9.8	4803.3	3.5	N/A	N/A
illite	0.5	5	-13.9	1054.9	2.2	40.2	-0.8
		7	-13.3	668.6	2.2	25.4	-0.5
		9	-13.9	557.7	2.2	26.8	-0.4
	1.0	5	-13.9	1529.3	2.2	73.4	-1.1
		7	-17.2	1044.3	2.2	99.5	-0.6
		9	-17.3	1009.0	2.2	96.2	-0.6
$nTiO_2$ + illite	0.5	5	21.6	5840.0	3.6	N/A	N/A
		7	2.0	3112.7	3.6	N/A	N/A
		9	-7.7	3814.7	3.6	0.7	-1.3
	1.0	5	28.0	5080.0	3.6	N/A	N/A
		7	1.8	5183.0	3.6	N/A	N/A
		9	5.3	3758.3	3.6	N/A	N/A
$nTiO_2$ + HA	0.5	5	-16.2	259.6	3.5	6.0	-0.2
		7	-16.2	252.6	3.5	5.8	-0.2
		9	-17.3	251.5	3.5	7.5	-0.2
	1.0	5	-16.0	288.7	3.5	2.6	-0.6
		7	-15.4	311.4	3.5	2.0	-0.7
		9	-16.8	322.9	3.5	4.1	-0.6
$nTiO_2$ + HA + illite	0.5	5	-16.2	520.2	3.6	12.0	-0.4
		7	-17.2	765.3	3.6	22.4	-0.6
		9	-17.5	485.3	3.6	15.2	-0.4
	1.0	5	-16.3	548.3	3.6	5.6	-1.1
		7	-15.9	595.5	3.6	5.0	-1.2
		9	-16.1	723.3	3.6	6.7	-1.5

At pH 9, the suspension was stable in 1 mM NaCl solution (Figure 1i), but unstable in 10 mM NaCl solution after 200 minutes (Figure 1j). In 1 mM NaCl solution, both illite and nTiO2 were negatively charged (-29.4 mV and -38.9 mV), resulting in high energy

barrier (221.8 k_BT) and electrostatic repulsion (Table 2). In 10 mM NaCl solution, illite and nTiO2 were also negatively charged (-29.9 mV and -34.1 mV), and the energy barrier was even higher (270.3 k_BT), which seemed to contradict the results of the stability test. The instability in 10 mM NaCl solution at pH 9 can be explained by the secondary minimum (-1.9 k_BT) (Table 2), which made HDD larger (1259 nm) and the suspension unstable. The effect of secondary minimum is discussed in detail in Section 3.7.

In $MgCl_2$ solutions, when illite and $nTiO_2$ co-existed, $nTiO_2$ exhibited instability at all pH (Figure 1k, 1l). At pH 5, the illite+$nTiO_2$ suspensions became unstable due to the attractive electrostatic forces between negatively-charged illite (-13.9 mV, Figure 2g) and positively-charged $nTiO_2$ (~ +30 mV, Figure 2f). At pH 7 and 9 in $MgCl_2$ solutions, as discussed previously, $nTiO_2$ suspensions themselves were unstable due to the low surface charge (Figure 2f). When negatively charged illite particles were mixed with these positively charged $nTiO_2$, the suspensions became even more unstable (Figure 1k, 1l). DLVO calculations confirmed no energy barriers between $nTiO_2$ and illite particles for all the pH (Table 3).

2.3.4 $nTiO_2$ stability in the presence of HA

In the presence of HA, in both 1 mM and 10 mM NaCl solutions, $nTiO_2$ was stable at all pH (Figure 1m, 1n). Unlike $nTiO_2$ suspensions, whose ZP at pH 5 and 7 were positive or near neutral, ZP of the $nTiO_2$+HA suspensions at pH 5 and 7 were negative (< -30 mV) (Figure 2d). At pH 9, ZP of the $nTiO_2$+HA suspension was negative, similar to that of the $nTiO_2$ suspension (< -30 mV) (Figure 2a and 2d). The negative ZP at pH 5 and 7 in the presence of HA was attributable to HA adsorption to $nTiO_2$. Previous studies showed that

at pH < $pH_{pcz, TiO2}$, $nTiO_2$ have high affinity for HA, and adsorption of HA to $nTiO_2$ changes particle zeta potential from positive to negative, while at pH > $pH_{pcz\ TiO2}$, $nTiO_2$ and HA both carry negative charges, and HA does not adsorb or influence the ZP of $nTiO_2$ (Wu and Cheng, 2016). DLVO calculations indicated that the energy barriers between $nTiO_2$ particles in the presence of HA were high (> 92 k_BT) (Table 2), in good agreement with the stability test results.

In $MgCl_2$ solutions, the presence of HA made $nTiO_2$ stable at all pH (Figure 1o, 1p). As discussed previously, $nTiO_2$ suspension in $MgCl_2$ solution was stable at pH 5 by itself due to the repulsive electrostatic forces between $nTiO_2$ particles, while at pH 7 and 9 $nTiO_2$ suspension was unstable due to the low net surface charges (Figure 2f). When HA was mixed with $nTiO_2$, all the $nTiO_2$ suspensions become negatively charged (-16 to -17 mV) (Figure 2i), attributable to HA adsorption to $nTiO_2$ (Erhayem and Sohn, 2014; Wu and Cheng, 2016). The calculated energy barriers between $nTiO_2$ particles in the $nTiO_2$+HA suspensions were low, ranging from 5.8 to 7.5 k_BT in 0.5 mM $MgCl_2$ solutions, and from 2.0 to 4.1 k_BT in 1 mM $MgCl_2$ solutions (Table 3). These energy barriers were only slightly higher than the kinetic energy of colloidal particles, but the suspensions showed good stability. Besides the calculated energy barriers, steric forces between HA-covered $nTiO_2$ particles can substantially enhance the repulsive forces (Chen et al., 2012), but were not included in the DLVO calculations. Thus the actual energy barriers could be higher than the calculated values.

2.3.5 $nTiO_2$ stability with co-existing illite particle and HA

In NaCl solutions, when both HA and illite particle were present together with $nTiO_2$,

the suspensions were stable for all the pH and IS (Figure 1q, 1r), and the ZP of the $nTiO_2$+HA+illite suspensions were all negative and comparable to those of the $nTiO_2$+HA suspensions (Figure 2e and 2d). As discussed previously, when HA and $nTiO_2$ were co-present, HA adsorption to $nTiO_2$ stabilized $nTiO_2$ particles, and made the ZP of $nTiO_2$ at pH 5 and 7 negative. When $nTiO_2$ particles became negatively charged, the attractive electrostatic forces between $nTiO_2$ and illite (as in the case of the $nTiO_2$+illite mixture) vanished, which prevented the formation of $nTiO_2$−illite aggregates and stabilized the suspension in the $nTiO_2$+HA+illite suspensions. DLVO calculations indicated high energy barriers in all the $nTiO_2$+HA+illite systems, consistent with the stability test results.

In $MgCl_2$ solutions, the $nTiO_2$+illite+HA mixtures were stable under all the tested conditions (Figure 1s, 1t). As discussed previously, HA adsorption to the positively-charged $nTiO_2$ changed the ZP of $nTiO_2$ from positive to negative (Figure 2i vs. Figure 2f), and therefore the interactive force between illite and $nTiO_2$ became repulsive. Compared to the ZP of the $nTiO_2$+illite+HA suspensions in the NaCl solutions (Figure 2e), the ZP in the $MgCl_2$ solutions (Figure 2j) were less negative, presumably due to higher adsorption and stronger screening effect of Mg^{2+}. The calculated energy barriers in the $MgCl_2$ solutions were also lower, but still high enough to maintain the stability of the suspension, i.e., the energy barriers were 12.0 to 22.4 k_BT in 0.5 mM $MgCl_2$ solutions, and 5.0 to 6.7 k_BT in 1 mM $MgCl_2$ solutions (Table 3). It should be noted again that steric force, which provided additional repulsion between particles, was not included in the calculation. Therefore the actual energy barrier should be higher than the calculated values.

It is also noted that $nTiO_2$ by itself carried positive charges in most of the $MgCl_2$ solutions (Figure 2f) and in NaCl solutions at pH 5 (Figure 2a), while both HA and illite

carried negative charges in these solutions (Figure 2b and 2g). Therefore, illite may compete against HA for $nTiO_2$ to form $nTiO_2$-illite aggregates, leading to unstable suspensions. However, all the $nTiO_2$+HA+illite suspensions were found stable, indicating that $nTiO_2$ in the mixed suspensions were mostly associated with HA. This is reasonable since HA adsorbs to $nTiO_2$ via chemical bonds, which are much stronger than the DLVO interactive forces. Additionally, when preparing the $nTiO_2$+HA+illite suspensions, $nTiO_2$ and HA were mixed before illite addition, which made the $nTiO_2$ negatively charged and prevented $nTiO_2$-illite association.

2.3.6 Particle size

The measured particle size (HDD) (Figure 3) in all cases were consistent with the results of the stability test and the DLVO calculated interaction energies, i.e., under the conditions where the suspensions were stable with large energy barrier between particles, the measured HDD were small (i.e., <1000 nm). For example, in NaCl solutions, the HDD of $nTiO_2$ were small at pH 5 (269 nm and 779 nm) and pH 9 (523 nm and 661 nm) (Figure 3a), indicating low degree of aggregation and stable suspension, in agreement with the stability test results (Figure 1a, 1b). Conversely, under the conditions where the suspensions were unstable with low or no energy barrier between particles, the HDD were large (i.e., >2000 nm). For example, when $nTiO_2$ were mixed with illite in the $MgCl_2$ solutions, the suspensions were unstable (Figure 1k, 1l) and the HDD were all very large (Figure 3h). The HDD were all small when HA was present (Figure 3d, 3e, 3i, 3j), attributable to the low degree of aggregation due to electrostaic and steric repulsion between HA-covered particles.

2.3.7 Role of secondary minimum

DLVO calculation indicated presence of secondary minimum under the conditions in some stability tests (mainly in 10 mM NaCl solutions, Table 2). E.g., the secondary minimum between $nTiO_2$ particles at pH 5 and 9 in 10 mM NaCl solution in the absence of HA and illite were -3.7 and -2.9 k_BT respectively. The magnitudes of these secondary minima were larger than the mean kinetic energy of colloidal particles (~1.5 k_BT) (Treumann et al., 2014) and therefore might cause particle aggregation and unstable suspension. However, our stability test showed that for all the cases where a secondary minimum was calculated, the suspensions were actually stable, except for the case of the $nTiO_2$+illite suspension at pH 9 in 10 mM NaCl solution.

It was noted that the HDD of the particles in these 10 mM NaCl solutions with a secondary minimum were larger than the HDD in 1 mM NaCl solutions with no secondary minimum. E.g., the HDD of $nTiO_2$ particles at pH 5 and 9 in 10 mM NaCl solution in the absence of HA and illite were 779 and 661 nm respectively, larger than those in 1 mM NaCl solutions (269 and 523 nm respectively at pH 5 and 9) (Figure 3a). The higher HDD in the 10 mM solutions confirmed particle aggregation in the presence of a secondary minimum. Furthermore, the HDD results showed that the particle aggregates in 10 mM NaCl solutions were small enough to remain suspended, therefore the suspensions were stable during the timespan of the experiment (Figure 1b). For the $nTiO_2$+illite suspension at pH 9 in 10 mM NaCl solution, the HDD was larger (1259 nm) (Figure 3c), and the suspension became unstable only after t > 200 minutes (Figure 1j). Due to the low magnitude of these secondary minima, the attractive forces caused by the secondary minimum are lower compared to those by the primary minima (i.e., the cases where there

is low or no energy barrier), therefore sizes of the aggregates were smaller and the suspensions were less unstable.

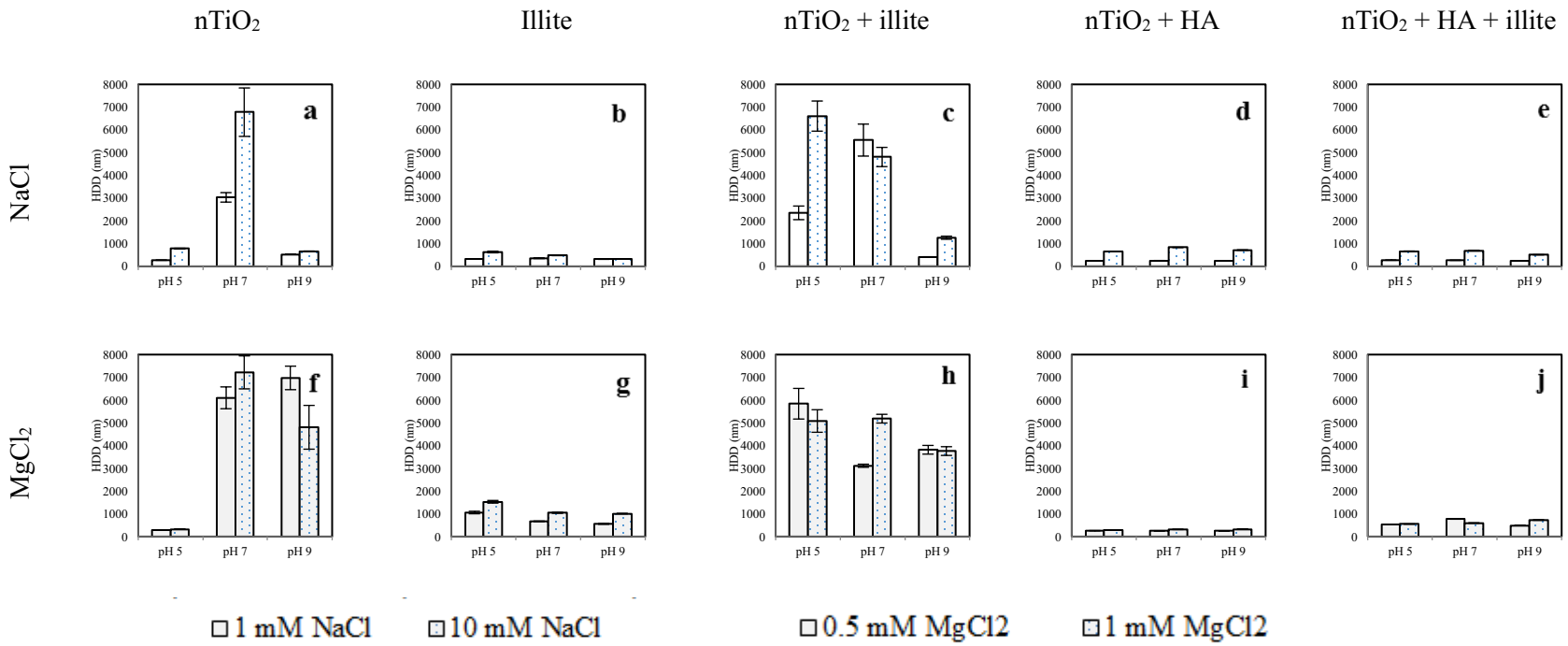

Figure 3. Hydrodynamic diameter (HDD) of the suspensions at pH 5, 7, and 9 in 1 mM NaCl (blank), 10 mM NaCl (spotted), 0.5 mM $MgCl_2$ (grey), and 1 mM $MgCl_2$ (grey soptted) solutions. Data is expressed as mean ± standard deviation of triplicate measurement.

2.4. Summary

Results from this study showed that in the absence of illite colloids and HA, ZP of $nTiO_2$ were generally more positive in $MgCl_2$ solutions than that in NaCl solutions at the same pH. This was caused by higher Mg^{2+} adsorption and stronger screening effect, both of which are due to the higher valence of Mg^{2+}. The cation valence effect was important at pH 7 and 9 where $nTiO_2$ became positive-charged in $MgCl_2$ solutions. When illite colloids and $nTiO_2$ particles co-existed, $nTiO_2$ were destabilized at pH < $pH_{pzc,TiO2}$ by illite colloids through formation of illite-$nTiO_2$ hetero-aggregates as a result of electrostatic attraction. At pH > $pH_{pzc,TiO2}$, illite colloids did not interfere with like-charged $nTiO_2$. Point of zero charge of $nTiO_2$ in $MgCl_2$ solution was higher than that in NaCl solution, and therefore hetero-aggregation in $MgCl_2$ solution occurred even at high pH. In both $MgCl_2$ and NaCl solutions, the presence of HA made $nTiO_2$ particles stable both in the absence and presence of illite colloids. This was caused by HA adsorption to positively-charged $nTiO_2$ particles, which made $nTiO_2$ surface negatively charged, and thus prevented the formation $nTiO_2$−$nTiO_2$ or illite−$nTiO_2$ aggregates. The measured HDD were in agreement with the stability test results, showing high degree aggregation (i.e., large HDD) in unstable suspensions and low degree aggregation in stable suspensions. The calculated interaction energy revealed that instability of the $nTiO_2$ suspensions was mainly caused by attractive electrostatic forces, which diminished energy barriers and resulted in rapid aggregation and sedimentation. Our results also

showed that secondary minima may exist in solutions with higher IS, and HDD measurement confirmed aggregation, however, the attractive forces caused by these secondary minima were low and therefore the suspensions were mostly stable during the timeframe of the tests. This study demonstrated that divalent cations, HA, and clay colloids all may interact with and remarkably influence the aggregation and stability of $nTiO_2$ particles, and their individual and synergistic effects must be considered for the specific chemical condition (e.g., pH, IS) in order to predict the fate and transport of $nTiO_2$ particles in natural aquatic environment.

Acknowledgments

This work was supported by Natural Sciences and Engineering Research Council of Canada's Discovery Grant (402815-2012) and Canada Foundation for Innovation's Leaders Opportunity Fund (31836).

2.5. References

Aiken, G. R., Hsu-Kim, H., Ryan, J. N. (2011). Influence of dissolved organic matter on the environmental fate of metals, nanoparticles, and colloids. Environ. Sci. Technol. 45, 3196−3201.

Alessi, D. S., Fein, J. B. (2010). Cadmium adsorption to mixtures of soil components: Testing the component additivity approach. Chemical Geology 270, 186–195.

Al-Kattan, A., Wichser, A., Zuin, S., Arroyo, Y., Golanski, L., Ulrich, A., Nowack, B. (2014). Behavior of TiO2 Released from Nano-TiO2 Containing Paint and Comparison to Pristine Nano-TiO2. Environ. Sci. Technol. 48, 6710–6718.

Amirianshoja, T., Junin, R., Idris, A. K., Rahmani, O. (2013). A comparative study of surfactant adsorption by clay minerals. Journal of Petroleum Science and Engineering 101, 21–27

Aruoja, V., Dubourguier, H., Kasemets, K., Kahru, A. (2009). Toxicity of nanoparticles of CuO, ZnO and TiO2 to microalgae Pseudokirchneriella subcapitata. Science of the Total Environment 407, 1461–1468.

Bergström, L. Hamaker constants of inorganic materials. (1997). Advances in Colloid and Interface Science 70, 125–169.

Boncagin, N. T., Otaegui, J. M., Warner, E., Curran, T., Ren, J., Fidalgo de Cortalezzi, M. M. (2009). Exchange of TiO_2 nanoparticles between streams and streambeds. Environ. Sci. Technol. 43, 7699–7705.

Bradl, H. B. (2004). Adsorption of heavy metal ions on soils and soils constituents. Journal of Colloid and Interface Science 277, 1–18.

Cai, L.; Tong, M.; Wang, X.; Kim, H. (2014). Influence of clay particles on the transport and retention of titanium dioxide nanoparticles in quartz sand. Environ. Sci. Technol. 48, 7323–7332.

Chen, G., Liu, X., Su, C. (2011). Transport and retention of TiO2 rutile nanoparticles in saturated porous media under low-ionic-strength conditions: measurements and mechanisms. Langmuir 27, 5393–5402.

Chen, G.; Liu, X.; Su, C. (2012). Distinct effects of humic acid on transport and retention of TiO2 Rutile Nanoparticles in saturated sand columns. Environ. Sci. Technol. 46, 7142–7150.

Chowdhury, I., Hong, Y., Honda, R. J., Walker, S. L. (2011). Mechanisms of TiO2 nanoparticle transport in porous media: Role of solution chemistry, nanoparticle concentration, and flow rate. Journal of Colloid and Interface Science 360, 548–555.

Coll, C., Notter, D., Gottschalk, F., Sun, T., Som, C., Nowack, B. (2015). Probabilistic environmental risk assessment of five nanomaterials (nano-TiO2, nano-Ag, nano-ZnO, CNT, and fullerenes). Nanotoxicology. Early Online: 1–9.

Domingos, R. F., Tufenkji, N., Wilkinson, j. k. (2009). Aggregation of Titanium Dioxide Nanoparticles: Role of a Fulvic Acid. Environ. Sci. Technol. 43, 1282–1286.

Dumat, C., Staunton, S. (1999). Reduced adsorption of caesium on clay minerals caused by various humic substances. Journal of Environmental Radioactivity 46, 187-200.

Erhayem. M., Sohn, M. (2014). Stability studies for titanium dioxide nanoparticles upon adsorption of suwannee river humic and fulvic acids and natural organic matter. Science of the Total Environment 468-469, 249–257.

Fang, J., Shan, X., Wen, B., Lin, J., Owens, G., Zhou, S. (2011). Transport of copper as affected by titanium nanoparticles in soil columns. Environmental Pollution 159, 1248–1256.

French, R. A., Jacobson, A. R., Kim, B., Isley, S. L., Penn, R. L., Baveye, P. C. (2009). Influence of ionic strength, pH, and cation valence on aggregation kinetics of titanium dioxide nanoparticles. Environ. Sci. Technol. 43, 1354–1359.

Gallego-Urrea, J. A., Holmberg, J. P., and Hassellöv, M. (2014). Influence of different types of natural organic matter on titania nanoparticle stability: effects of counter ion concentration and pH. Environ. Sci. Nano. 1, 181–189.

Gregory, J. (1981). Approximate expressions for retarded van der waals interaction. J. Colloid Interface Sci. 83, 138-145.

Gómez-Merino, A. I., Rubio-Hernández, F. J., Velázquez-Navarro, J.F., Galindo-Rosales, F.J., Fortes-Quesada, P. (2007). The Hamaker constant of anatase aqueous suspensions, Journal of Colloid and Interface Science 316, 451–456.

Gondikas, A. P., Kammer, F., Reed, R. B., Wagner, S., Ranville, J. F., Hofmann, T. (2014). Release of TiO_2 Nanoparticles from Sunscreens into Surface Waters: A One-Year Survey at the Old Danube Recreational Lake. Environ. Sci. Technol. 48, 5415–5422.

Heinlaan, M., Ivask, A., Blinova, I., Dubourguier, H. C., Kahru, A. (2008). Toxicity of nanosized and bulk ZnO, CuO and TiO_2 to bacteria Vibrio fischeri and crustaceans Daphnia magna and Thamnocephalus platyurus. Chemosphere 71, 1308–1316.

Hiemenz, P. C., Rajagopalan, R. (1997). Principles of colloid and surface chemistry, 3rd Ed. Marcel Dekker, Inc. New York.

Israelachvili, J. N. (2011). Intermolecular and surface forces (3rd ed). California, Academic Press.

Jiang, M., Jin, X., Lu, X., Chen, Z. (2010). Adsorption of Pb(II), Cd(II), Ni(II) and Cu(II) onto natural kaolinite clay. Desalination 252, 33–39.

Jung, B., O'Carroll, D., Sleep, B. (2014). The influence of humic acid and clay content on the transport of polymer-coated iron nanoparticles through sand. Science of the Total Environment 496, 155–164.

Lee, J., Bartelt-Hunt, S., Li, Y., Gilrein, E. (2016). The influence of ionic strength and organic compounds on nanoparticle TiO_2 (n-TiO_2) aggregation. Chemosphere 154, 187–193.

Liu, X., Wazne, M., Han, Y., Christodoulatos, C., Jasinkiewicz, K. L. (2010). Effects of natural organic matter on aggregation kinetics of boron nanoparticles in monovalent and divalent electrolytes. Journal of Colloid and Interface Science 348, 101–107.

Liu, X., Wazne, M., Chou, T., Xiao, R., Xu, S. (2011). Influence of Ca^{2+} and Suwannee River Humic Acid on aggregation of silicon nanoparticles in aqueous media. Water Research 45, 105–112.

Long, J., Xu, Z., Masliyah, J. H. (2006). Role of illite–illite interactions in oil sands processing. Colloids and Surfaces A: Physicochemical and Engineering Aspects 281, 202–214.

Loosli, F., Le Coustumer, P., Stoll, S. (2013). TiO_2 nanoparticles aggregation and disaggregation in presence of alginate and Suwannee River humic acids. pH and concentration effects on nanoparticle stability. Water Research 47, 6052–6023.

Loosli, F., Le Coustumer, P., Stoll, S. (2015). Effect of electrolyte valency, alginate concentration and pH on engineered TiO_2 nanoparticle stability in aqueous solution. Science of the Total Environment 535, 28–34.

Ludwig, C., Schindler, P. W. (1995). Surface Complexation on TiO_2: I. Adsorption of H+ and Cu^{2+} Ions onto TiO_2 (Anatase). Journal of Colloid and Interface Science 169. 284–290.

Nebbioso, A., Piccolo, A. (2013). Molecular characterization of dissolved organic matter (DOM): a critical review. Anal Bioanal Chem. 405,109–124.

Novich, B. E., Ring, T. A. (1984). Colloid stability of clays using photon correlation spectroscopy. Clays and Clay Minerals 32, 400–406.

Nowack, B., Bucheli, T. D. (2007). Occurrence, behavior and effects of nanoparticles in the environment. Environmental Pollution 150, 5–22.

Rashid, M. A., Buckley, D. E., Robertson, K. R. (1972). Interactions of a marine humic acid with clay minerals and a natural sediment. Geoderma 8, 11-27.

Torkzaban, S., Wan, J., Tokunaga, T. K., Bradford, S. A. (2012). Impacts of bridging complexation on the transport of surface-modified nanoparticles in saturated sand. Journal of Contaminant Hydrology 136–137, 86–95.

Treumann, S., Torkzaban, S., Bradford, S. A., Visalakshan, R. M., Page, D. (2014). An explanation for differences in the process of colloid adsorption in batch and column studies. Journal of Contaminant Hydrology 164, 219–229.

Van Olphen, H. (1963). An Introduction to Clay Colloid Chemistry. Interscience, New York.

Wang, Q., Cheng, T., Wu, Y. (2015). Distinct roles of illite colloid and humic acid in mediating arsenate transport in water-saturated sands columns. Water Air Soil Pollut. 226: 129.

Wang, H., Dong, Y., Zhu, M., Li, X., Keller, A. A., Wang, T., Li, F. (2015). Heteroaggregation of engineered nanoparticles and kaolin clays in aqueous environments. Water Research 80, 130–138.

Wang, D., Zhang, W., Zhou, D. (2013). Antagonistic effects of humic acid and iron oxyhydroxide grain-coating on biochar nanoparticle transport in saturated sand. Environ. Sci. Technol. 47, 5154–5161.

Wilson, M. J., Wilson, L., Patey, I. (2014). The influence of individual clay minerals on formation damage of reservoir sandstones: a critical review with some new insights. Clay Miner. 49, 147–164.

Wu, Y., Cheng, T. (2016). Stability of $nTiO_2$ particles and their attachment to sand: Effects of humic acid at different pH. Science of the Total Environment 541, 579–589.

Zhang, Y., Cheng, Y., Westerhoff, P., Crittenden, J. (2009). Impact of organic matter and divalent cations on the stability of aqueous nanoparticles. Water Research 43, 4249–4257.

Zhou, D., Abdel-Fattah, A. I., Keller, A. A. (2012). Clay Particles Destabilize Engineered Nanoparticles in Aqueous Environments. Environ. Sci. Technol. 46, 7520−7526.

Chapter 3: Concurrent aggregation and deposition of nanoscale titanium dioxide ($nTiO_2$) in the presence of clay colloids

Abstract

Although extensive research has been conducted to investigate $nTiO_2$ aggregation and deposition, concurrent aggregation and deposition of $nTiO_2$, which has important implications to the fate and transport of $nTiO_2$ in groundwater, has received only limited attention. The objective of this study is to investigate how pH, dissolved organic matter, and Fe/Al oxyhydroxide coatings influence aggregation and simultaneous deposition of $nTiO_2$. Experiments were performed to examine $nTiO_2$ aggregation and deposition onto a quartz sand with co-present illite, kaolinite, and montmorillonite colloids under various geochemical conditions. Results showed that $nTiO_2$ formed hetero-aggregates (i.e., $nTiO_2$-clay aggregates) when $nTiO_2$ and the clay colloids carried opposite charges, and the hetero-aggregates may either deposit or remain suspended depending on their interactions with quartz sand and Fe/Al oxyhydroxide coatings. Deposition of $nTiO_2$ and/or $nTiO_2$+clay aggregates occurred when there were Mg^{2+} bridging, electrostatic attraction, or secondary minimum. Humic acid was found to prevent $nTiO_2$ aggregation and deposition under most conditions. In $MgCl_2$ solutions, however, it facilitated deposition by adsorbing to $nTiO_2$ and Fe/Al oxyhydroxides and thereby enabling Mg^{2+} bridging. This study demonstrated the important and complex role clay colloids may play in concurrent aggregation and transport of $nTiO_2$.

Keywords: Nanoscale titanium dioxide ($nTiO_2$); Clay colloids; Fe/Al oxyhydroxide coated quartz sand; Concurrent aggregation and deposition; Zeta potential (ZP) and hydrodynamic diameter (HDD); DLVO interaction energy

3.1. Introduction

Nanoscale titanium dioxide particles ($nTiO_2$) is a widely used engineered nano-material and extensive research has been conducted to understand its fate and transport in the environment due to the potential risks $nTiO_2$ may pose to ecosystems and human health (Skocaj et al., 2011). Deposition is a primary process that controls $nTiO_2$ transport in groundwater (Godinez and Darnault, 2011; Cai et al., 2014), by which $nTiO_2$ is attached to sediment grain and removed from water. Aggregation is another important process that influence $nTiO_2$ transport, by which smaller particles attract to each other to form larger aggregates that are susceptible to gravity sedimentation and physical straining (Chen et al., 2011). It is well established that water chemistry and components could have remarkable influence on $nTiO_2$ aggregation and deposition. While neutral pH, high ionic strength, and multivalent cations are found to promote homo-aggregation of $nTiO_2$ (Chen et al., 2011; Loosli et al., 2013; Wu and Cheng, 2016; Tang and Cheng, 2018), dissolved natural organic matter (DOM) normally hinders $nTiO_2$ aggregation via absorbing onto $nTiO_2$ and intensifying the negative charges on particle surface (Erhayem and Sohn, 2014; Wu and Cheng, 2016; Tang and Cheng, 2018). $nTiO_2$ deposition in porous media is also affected by water chemistry. High pH, low ionic strength, and DOM generally impede $nTiO_2$ deposition, while low pH, high ionic strength, and multivalent cations (e.g., Ca^{2+}, Mg^{2+}) are found to enhance deposition (Chen et al., 2011; Han et al., 2014; Xu et al., 2017).

Water-borne clay colloids, a common groundwater component, could have significant effect on $nTiO_2$ aggregation and deposition. Clay minerals carry negative charges in natural groundwater due to their low point of zero charge (PZC) (Sposito, 1984refs). $nTiO_2$, in contrast, has a PZC near neutral pH (Tang and Cheng, 2018; Wu and Cheng, 2016), and carry positive charges in low pH water. Under conditions where $nTiO_2$ and clay are oppositely charged, hetero-aggregates between $nTiO_2$ and water-borne clay colloids will form (Zhou et al., 2012; Valera-Zaragoza et al., 2014; Tang and Cheng, 2018). Particle surface charge is influenced by pH, ionic strength, cation valence, and DOM, therefore the formation of $nTiO_2$-clay aggregates is affected by all the above factors. It is reported that low pH, high ionic strength, and multivalent cations (e.g., Ca^{2+} and Mg^{2+}) promote the formation of $nTiO_2$-clay aggregates, and high pH, low ionic strength, and DOM hinders such aggregation (Tang and Cheng, 2018).

Although much work has been conducted to investigate $nTiO_2$ aggregation and deposition, concurrent aggregation and deposition of $nTiO_2$ have been examined only in a few studies. In porous media, nanoparticles may form aggregates during transport, and the formation of aggregates could further alter nanoparticle deposition and transport (Wiesner and Bottero 2007). Solovitch et al. (2010) found that the rate of $nTiO_2$ homo-aggregation in pore water may comparable to that of deposition, and formation of the aggregates enhances $nTiO_2$ deposition. However, the aggregates that are not deposited will move faster than the smaller $nTiO_2$ due to size

exclusion effect. Cai et al. (2014) reported that in dilute NaCl solutions, mobility of $nTiO_2$ in quartz sand column is enhanced in the co-presence of suspended bentonite and kaolinite colloids. This higher mobility is attributable to the formation of $nTiO_2$-bentonite and $nTiO_2$-kaolinite hetero-aggregates, which have lower deposition rate and therefore higher mobility compared to $nTiO_2$. In contrast, the mobility of $nTiO_2$ in dilute $CaCl_2$ solutions with the co-presence of suspended kaolinite colloids is lower than $nTiO_2$ alone, which is attributable to the straining of the larger but less negatively charged $nTiO_2$-kaolinite aggregates. The aforementioned studies have shown the important implications of concurrent aggregation and deposition to the fate and transport of $nTiO_2$, and provided valuable insights into the mechanisms involved in such process. However, a number of critical issues have not been addressed. pH and DOM are two key factors that control $nTiO_2$ hetero-aggregation in the presence of clay colloids (Tang and Cheng, 2018), yet, their influence on concurrent aggregation and deposition has not been examined. Fe and Al oxyhydroxide coatings are common constituents of sediment grains and may substantially alter nanoparticle deposition (Liu et al., 2012). Yet, deposition of $nTiO_2$ homo- and hetero-aggregates has not been studied using media other than pure quartz sand.

This study was designed to fill the gaps by studying the influence of pH, DOM, and Fe/Al oxyhydroxide coatings on concurrent aggregation and deposition of $nTiO_2$ in the presence of clay colloids. Batch experiments were performed to study $nTiO_2$ aggregation and deposition onto a

quartz sand with trace amount of metal oxyhydroxide coatings. Illite, kaolinite, and montmorillonite colloids were chosen as representing clay colloids due to their abundance in natural groundwater and the disparity in their surface charge density (Wainipee et al., 2013). Three background electrolyte solutions (3 mM NaCl, 0.1 mM and 1 mM $MgCl_2$) at pH 5 and 9 were tested to elucidate the effect of pH and cation valance and concentration. Based on the experimental measurements and the interaction energy calculated using DLVO (Derjaguin-Landau-Verwey-Overbeek) theory, mechanisms of concurrent aggregation and deposition of $nTiO_2$ under different geochemical conditions were proposed.

3.2. Materials and Methods

3.2.1. Materials

Particle suspensions. To prepare $nTiO_2$ suspension, Aeroxide™ TiO_2 P25 powder with >99.5+ purity (Fisher Scientific) was weighed using an analytical balance, and suspended in background solution prepared using ACS reagent grade NaCl or $MgCl_2$ (VWR Internal) and nanopure water. The $nTiO_2$ suspension was sonicated using a Branson Digital Sonifier (Crystal Electronics) for 30 min with 120 W power. pH of the suspension was measured by a pH meter (Orion star A211, Thermo Scientific) and adjusted to 5 or 9 by adding small volumes of 0.1 M NaOH and 0.1 M HCl.

Clay colloid stock suspensions were prepared by suspending 4-gram clay powder (The Clay Mineral Society) in 1000 mL nanopure water and sonicating using a Branson Digital Sonifier for 60 min with 200 W power. The suspensions were then let stand for 24 hours to allow large particles to settle before the supernatant was carefully transferred to a high-density polyethylene bottle. To determine particle concentration in the suspension, 100 mL well mixed suspension was filtered through a 0.1 μm polyethersulfone membrane filter (Pall Life Sciences). The filter was oven dried at 60 ℃ and the weight difference of the filter before and after filtration was used to calculate particle concentration.

To prepare humic acid (HA) stock solution, 100 mg HA powder (Alfa Aesar) was weighed and dissolved in 100 mL nanopure water, and stored in darkness at 4 ℃ for subsequent use.

Quartz sand. Quartz sand (U.S. Silica) was sieved to a size range of 0.250-0.355 mm, soaked in 0.1 M NaOH and 0.1 M HCl solutions respectively overnight, rinsed with nanopure water multiple times, and dried in oven at 100 ℃. According to the manufacturer, the sand is predominantly composed of pure quartz, with trace levels of impurities like Fe and Al oxyhydroxides. SEM-EDX analysis was used to confirm the mineralogy, and SEM-EDX used to determine trace elements (if any) in the sand. Acid digestion plus ICP-MS analysis was used to quantify metal concentration (if any) of the sand.

To measure zeta potential of the quartz sand, the sand was crushed into powder and 4-grams sand powder was suspended in 1000 mL 3 mM NaCl, 0.1 mM and 1 mM $MgCl_2$ background solution respectively and sonicated for 60 min with 200 W power. Then the suspensions were let stand for 24 hours to settle down large particles, and supernatant samples were taken and diluted using background solutions. HA was added to some of the samples to achieve a HA concentration of 3 mg/L. pH of the samples was adjusted the to 5 and 9 by adding small volumes of 0.1 M NaOH or 0.1 M HCl before zeta potential was measured on a zetasizer (Zetasizer Nano ZS, Malvern).

3.2.2. $nTiO_2$ aggregation and deposition

$nTiO_2$ aggregation and deposition. Batch experiments were conducted to study $nTiO_2$ aggregation and deposition. The components ($nTiO_2$, clay particle, and HA) and their concentrations in the experiments are shown in Table 4 (Suspension type 1−8). In each experiment, clay stock suspension and HA stock solution were mixed with freshly prepared $nTiO_2$ suspension to achieve the desired concentration. The mixed suspensions were sonicated for 30 min with 120 W power to disperse the particles, and pH of the sample was adjusted by adding small volumes of 0.1 M NaOH and 0.1 M HCl solution.

After pH adjustment, 100 mL suspension was immediately mixed with 75 g quartz sand in 125 mL high-density polyethylene bottles, and pH was adjusted again to 5 or 9. Then the bottles were shaken at a speed of 120 rpm for 4 hours on a standard analog shaker (VWR International).

Table 4. $nTiO_2$, clay colloids, and humic acid (HA) concentration in the particle suspensions

Suspension type*	Components	$nTiO_2$ concentration (mg/L)	Illite concentration (mg/L)	Kaolinite concentration (mg/L)	Montmorillonite concentration (mg/L)	HA concentration (mg/L)
1	$nTiO_2$	50	-	-	-	-
2	$nTiO_2$+illite	50	10	-	-	-
3	$nTiO_2$ +kaolinite	50	-	10	-	-
4	$nTiO_2$+montmorillonite	50	-	-	10	-
5	$nTiO_2$+HA	50	-	-	-	3
6	$nTiO_2$+illite+HA	50	10	-	-	3
7	$nTiO_2$+kaolinite+HA	50	-	10	-	3
8	$nTiO_2$+montmorillonite+HA	50	-	-	10	3
9	illite	-	10	-	-	-
10	kaolinite	-	-	10	-	-
11	montmorillonite	-	-	-	10	-

*Each type of suspension was prepared in three types of background solution (i.e., 3 mM NaCl, 0.1 mM $MgCl_2$ and 1 mM $MgCl_2$), and for each type of background solution, two pH (i.e., 5 and 9) were tested.

All the experiments were performed in duplicate. The absorbance of the particle suspensions was measured at t = 0, 30, 60, 120, 180, and 240 minutes using a UV-Vis spectrophotometer (Genesys 10S UV-Vis, Thermo Scientific). During the experiment, small volumes of 0.1 M NaOH or HCl were added into the bottles when necessary to maintain the pH at 5 or 9. For each measurement, the bottle was removed from the shaker and let stand for 30 seconds to allow the sand grains to settle before supernatant sample was taken for absorbance measurement. A wavelength of 600 nm was used for measuring the absorbance, since at this wavelength, light absorbance is high for $nTiO_2$ but low for clay colloids and HA (Cai et al., 2014; Tang and Cheng, 2018). Our preliminary tests confirmed that, for the clay colloids, $nTiO_2$, and HA concentrations used in the experiments, the absorbance of clay colloids and HA was negligible at this wavelength (Fig. S1, SI).

Sand blank control. Sand blank control experiments were performed using the same procedure as described above. In the control experiments, no sand was used, and concentrations of $nTiO_2$, clay colloids, and HA, and the background electrolyte type and pH were the same as those for $nTiO_2$ aggregation and deposition experiments (Suspension type 1−8, Table 1).

Hydrodynamic diameter (HDD) and zeta potential (ZP) measurement. Particle suspensions (Suspension type 1−11, Table 1) were prepared using the same protocol as that in the sand blank control experiments. After 2 hours shaking, hydrodynamic diameter (HDD) and zeta potential (ZP) of the particle suspensions were measured on a zetasizer (Zetasizer Nano ZS, Malvern).

3.2.3. Calculation of interaction energy

DLVO (Derjaguin-Landau-Verwey-Overbeek) theory (Van Olphen, 1963) was used to calculate the DLVO forces between particle and particle and between particle and quartz sand. By assuming sphere geometry for particles, Equation (1) and (2) can be used to calculate the London-van der Waals (LW) force and electric double layer (EDL) force between two particles, and Equation (3) and (4) to calculate the LW and EDL forces between a particle and sand surface (Gregory, 1981, Chen et al., 2011). The overall DLVO force is the sum of the LW and EDL forces.

$$\emptyset_{\mathrm{LW}} = -\frac{\mathrm{AR_1R_2}}{6\mathrm{D}(\mathrm{R_1}+\mathrm{R_2})}\left[1-\frac{5.32D}{\lambda}\ln\left(1+\frac{\lambda}{5.32D}\right)\right]^{-1} \quad (1)$$

$$\emptyset_{\mathrm{EDL}} = \frac{2\pi \mathrm{R_1R_2}n_\infty k_B T}{(\mathrm{R_1}+\mathrm{R_2})\kappa^2}\left(\psi_1{}^2+\psi_2{}^2\right)\left\{\frac{2\psi_1\psi_2}{\psi_1{}^2+\psi_2{}^2}\ln\left[\frac{1+\exp(-\kappa \mathrm{D})}{1-\exp(-\kappa \mathrm{D})}\right]+\ln[1-\exp(-2\kappa \mathrm{D})]\right\} \quad (2)$$

$$\emptyset_{\mathrm{LW}} = -\left(\frac{\mathrm{AR}}{6\mathrm{D}}\right)\left[1+\left(\frac{14\mathrm{D}}{\lambda}\right)\right]^{-1} \quad (3)$$

$$\emptyset_{\mathrm{EDL}} = \pi\varepsilon_0\varepsilon_{\mathrm{r}}\,\mathrm{R}\left\{2\psi_c\psi_s\ln\left[\frac{1+\exp(-\kappa \mathrm{D})}{1-\exp(-\kappa \mathrm{D})}\right]+\left(\psi_c{}^2+\psi_s{}^2\right)\ln[1-\exp(-2\kappa \mathrm{D})]\right\} \quad (4)$$

where A (J) is Hamaker constant, R_1, R_2 and R (m) are particle radius, D (m) is separation distance, λ is the characteristic wavelength of interaction (10^{-7} m), ε_0 (8.85×10^{-12} $C^2J^{-1}m^{-1}$) is the permittivity of vacuum, ε_r (80) is the relative dielectric constant of the medium, n_∞ is number concentration of the bulk ion, κ (m^{-1}) is the Debye–Hückel reciprocal length, and $\kappa = 2.32\times10^9\ (\Sigma C_i Z_i^2)^{1/2}$, where C_i is the concentration of ion i (L^{-1}) and Z_i is the valency value. ψ_1 (V), ψ_2 (V) and ψ_c (V) are zeta potential of the particles, and ψ_S (V) is zeta potential of quartz surface.

To estimate the DLVO forces between $nTiO_2$ and clay colloids in $nTiO_2$+clay suspensions with no HA, ZP and HDD measured on $nTiO_2$ and clay suspensions in the same background solution and pH were used. To calculate the DLVO forces between $nTiO_2$ and clay colloids in $nTiO_2$+clay+HA suspensions, ZP and HDD measured on $nTiO_2$+HA suspensions, and ZP and HDD measured on clay suspensions were used, since adsorption of humic substances to $nTiO_2$ is high and therefore ZP and HDD of $nTiO_2$ are influenced by HA (Tang and Cheng, 2018). In contrast, adsorption of humic substances to clay colloids is negligibly low (Feng et al., 2005) and hence ZP and HDD of clay colloids are not affected by HA.

The Hamaker constant (A) used for $nTiO_2$-water-$nTiO_2$ was 3.5×10^{-20} J (Gómez-Merino et al., 2007), and for $nTiO_2$-water-kaolinite, $nTiO_2$-water-illite, and $nTiO_2$-water- montmorillonite were 3.9×10^{-20} J, 3.6×10^{-20} J, and 3.3×10^{-20} J respectively, calculated using Equation (5) (Hiemenz, 1997).

$$A_{132} = (\sqrt{A_{11}} - \sqrt{A_{33}})(\sqrt{A_{22}} - \sqrt{A_{33}}) \quad (5)$$

where 1 is $nTiO_2$, 2 is clay, and 3 is water. And the following constants, $A_{TiO2\text{-}TiO2}$ = 1.53×10^{-19} J (Bergström, 1997), $A_{H2O\text{-}H2O}$ = 3.7×10^{-20} J (Israelachvili, 2011), $A_{kaolinite\text{-}kaolinite}$ = 1.5×10^{-19} J, $A_{illite\text{-}illite}$ = 1.4×10^{-19} J, $A_{montmorillonite\text{ - }montmorillonite}$ = 1.3×10^{-19} J (Novich & Ring, 1984), was used as A_{22}.

For the particle-water-quartz systems, $A_{nTiO2\text{-}H2O\text{-}quartz} = 1.4\times10^{-20}$ J (Butt et al., 2005) was used to quantify the DLVO forces between $nTiO_2$ and quartz surface. The Hamaker constants for calculating the DLVO forces between $nTiO_2$-clay aggregates and quartz surface are difficult to constrain, therefore we used two end members, i.e., $A_{nTiO2\text{-}H2O\text{-}quartz} = 1.4\times10^{-20}$ J and $A_{clay\text{-}H2O\text{-}quartz} = 0.55\times10^{-20}$ J (Israelachvili, 2011), to estimate the range. According to Israelachvili (2011), a uniform Hamaker constant $A_{clay\text{-}H2O\text{-}quartz} = 0.55\times10^{-20}$ J can be used for different types of clays. The ZP and HDD measured on the $nTiO_2$+clay and $nTiO_2$+clay+HA suspensions were used as the ZP and HDD the $nTiO_2$+clay aggregates in the calculation.

3.3. Results and Discussion

3.3.1. $nTiO_2$ aggregation

3.3.1.1. $nTiO_2$ aggregation in the absence of HA

In 3 mM NaCl solution. The $nTiO_2$+kaolinite, $nTiO_2$+illite, and $nTiO_2$+montmorillonite suspensions with no HA at pH 5 showed very large HDD (>3000 nm) (Figure 4b), suggesting particle aggregation. The aggregation in these suspensions was caused by the attractive electrostatic forces between positively charged $nTiO_2$ and negatively charged clay colloids (Figure 5a). DLVO calculation confirmed no energy barriers between $nTiO_2$ and each of the clay particles (Table 5), suggesting that hetero-aggregates should form.

For the $nTiO_2$ suspension with no HA at pH 5, and for all the four suspensions with no HA at pH 9, the HDD was small (<900 nm) (Figure 4a & 4b), indicating stable suspensions. This was consistent with the measured ZP, which showed that the particles in these suspensions were either positively charged ($nTiO_2$ suspension at pH 5) (Figure 5a), or negatively charged (all the suspensions at pH 9) (Figure 5a). Therefore, repulsive electrostatic forces existed between the $nTiO_2$ particles and between $nTiO_2$ and clay particles. DLVO calculation confirmed high energy barriers and no secondary minima in these suspensions (Table 5), indicating that the net force between particles was repulsive and the suspensions should be stable.

In 0.1 mM $MgCl_2$ solution. In the absence of HA, high HDD (>3000 nm) was observed for the $nTiO_2$+illite and $nTiO_2$+montmorillonite suspensions at pH 5, and all the suspensions at pH 9

(Figure 4e). The aggregation at pH 5 was caused by the formation of $nTiO_2$-clay hetero-aggregates, as the $nTiO_2$ and clay colloids carried opposite charges in these suspensions (Figure 5d), and DLVO calculation showed no energy barriers between $nTiO_2$ and illite or montmorrillonite particles (Table 6). At pH 9, DLVO calculation showed no energy barriers between $nTiO_2$ particles in the $nTiO_2$ suspension (Table 6). This was due to the weak electrostatic charges (ZP = -9.4 mV) of $nTiO_2$, which resulted in weak electrostatic repulsive force that was lower than the van der waals force. As a result, the net force was always attractive between the $nTiO_2$ particles. Additionally, due to the high affinity of TiO_2 for cations at high pH (Tamura et al., 1996), it is very likely that Mg^{2+} could bridge negatively charged $nTiO_2$ particles and promote aggregation. For the $nTiO_2$+kaolinite, $nTiO_2$+illite, and $nTiO_2$+montmorillonite suspensions at pH 9, $nTiO_2$ and each of the clay colloids carried negative charges (Figure 5d), and DLVO calculation showed energy barriers between $nTiO_2$ and clay particle (Table 6), suggesting that no hetero-aggregation should occur. The large HDD observed in these suspensions, therefore, was the result of homo-aggregation of the $nTiO_2$ particles.

For the $nTiO_2$ suspension at pH 5, its ZP was positive (ZP = 36.1 mV) and DLVO calculation showed high energy barrier (160.4 k_BT) between $nTiO_2$ particles (Table 6), indicating no aggregation, which was consistent with the small HDD observed (624 nm). For the $nTiO_2$+kaolinite suspension at pH 5, the $nTiO_2$ and kaolinite carried opposite charges (Figure 5d),

and DLVO calculation showed no energy barriers between $nTiO_2$ and kaolinite particle. Therefore, hetero-aggregation was expected. However, the HDD of the $nTiO_2$+kaolinite suspension was small (295 nm), suggesting no aggregation. The discrepancy between DLVO calculation and experimental results was probably caused by the hydrodynamic forces during shaking. Due to the weak negative charges on kaolinite (ZP = -6.1 mV), the attractive force between $nTiO_2$ and kaolinite was low, and therefore, its effect on particle aggregation could be offset by the relatively strong hydrodynamic forces in agitated batch systems.

In 1 mM $MgCl_2$ solution. In the absence of HA, large HDD (>4000 nm) was observed for the $nTiO_2$+illite and $nTiO_2$+montmorillonite suspensions at pH 5 (Figure 4h), and all the four suspensions at pH 9 (Figure 4h). The mechanisms of aggregation at pH 5 was similar to those in 0.1 mM $MgCl_2$ solution. i.e., positively charged $nTiO_2$ and negatively charged clay colloid (Figure 5g) attracted to each other and formed hetero-aggregates. At pH 9, aggregation mechanisms were also similar to that in 0.1 mM $MgCl_2$ solution, i.e., due to the weak charges on $nTiO_2$ (ZP = 3.5 mV) (Figure 5g), no energy barrier existed between $nTiO_2$ particles (Table 7), resulting in homo-aggregation. In 1 mM $MgCl_2$ solution at pH 9, the $nTiO_2$ was positively charged (Figure 5g), therefore bridging of $nTiO_2$ by Mg^{2+} was not likely. However, the positively charged $nTiO_2$ could be attracted by the negatively charged clay colloids (Figure 5g) to form hetero-aggregates.

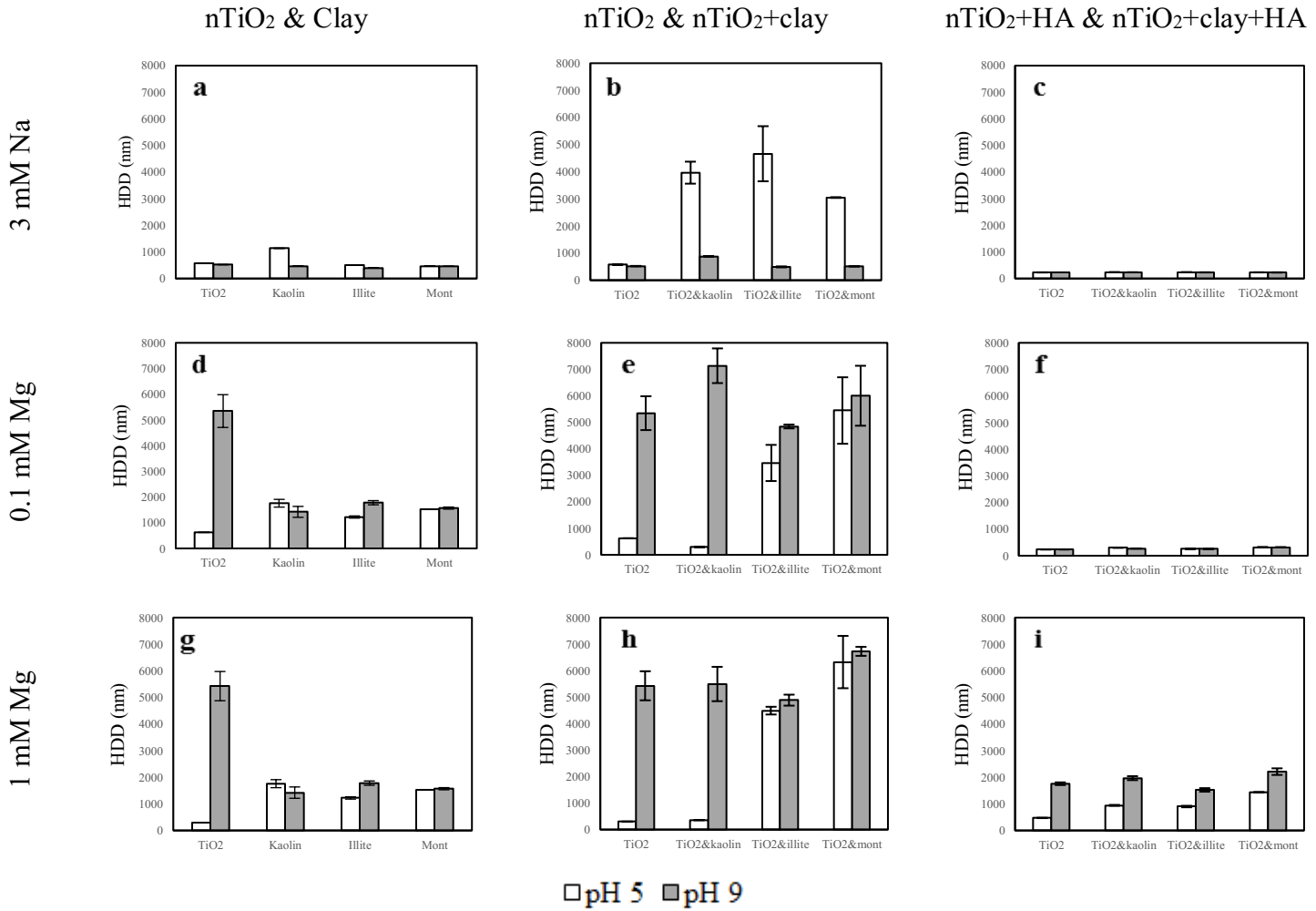

Figure 4. Hydrodynamic diameter (nm) of mixing and solo NPs & Clay at pH 5 & 9 in 3 mM NaCl, 0.1 mM and 1 mM $MgCl_2$ solutions. *Kaolin means kaolinite, and mont means montmorillonite. The data of $nTiO_2$ are presented in 'Solo $nTiO_2$ and Clay' section as well as '$nTiO_2$ & Clay'.

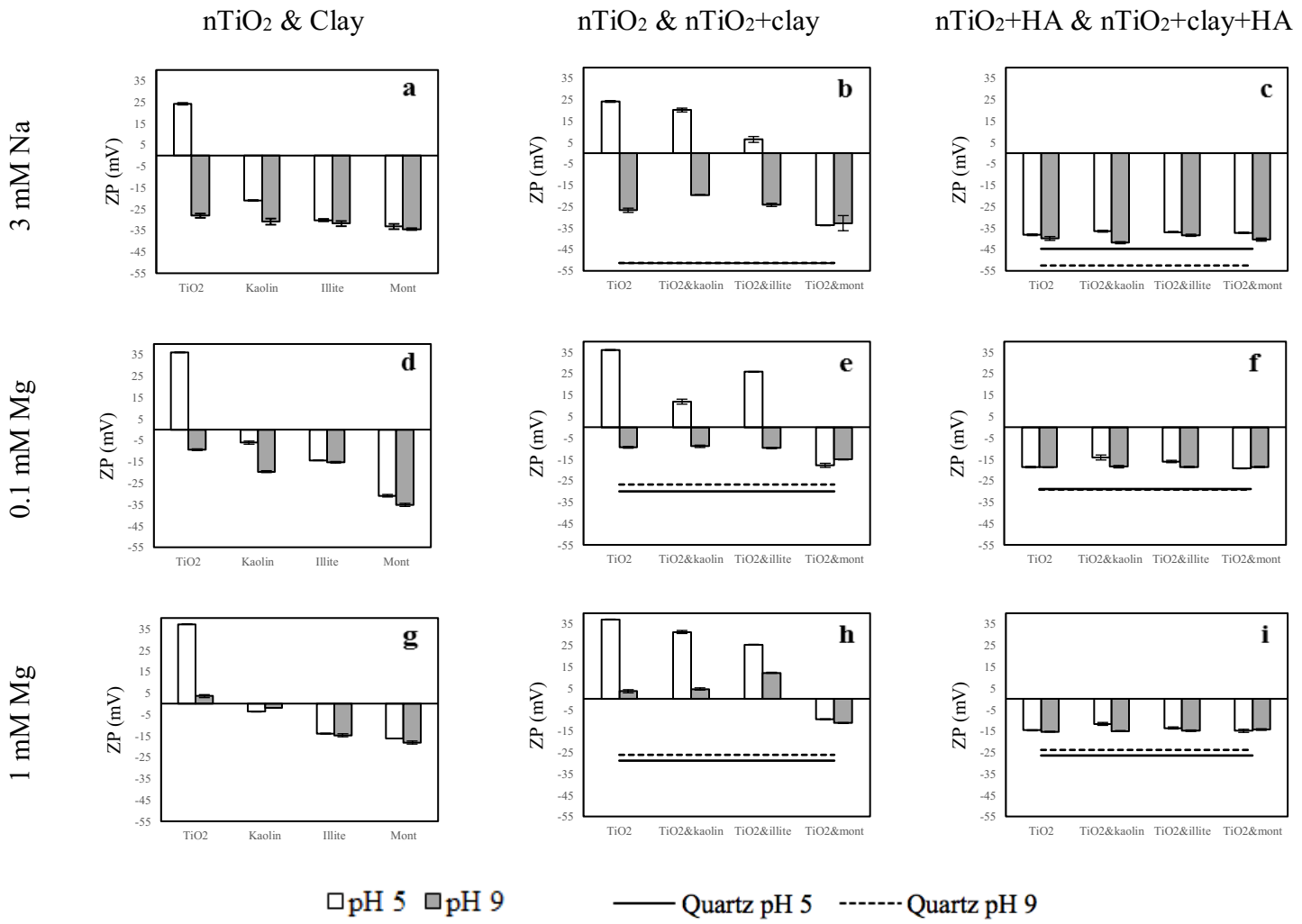

Figure 5. Zeta potential (mV) of quartz sand, mixing and solo NPs & Clay at pH 5 & 9 in 3 mM NaCl, 0.1 mM and 1 mM $MgCl_2$ solutions. *Kaolin means kaolinite, and mont means montmorillonite. The data of $nTiO_2$ are presented in 'Solo $nTiO_2$ and Clay' section as well as '$nTiO_2$ & Clay'.

Table 5. The pH, Zeta Potential (ZP), and Hydrodynamic Diameter (HDD) of the suspensions in 3mM NaCl solutions, and the Energy Barrier ($\emptyset_{max}$) and Secondary Minimum ($\emptyset_{2min}$) calculated for the particle-particle interaction based on DLVO theory

pH	Suspension	ZP of $nTiO_2$ (clay) (mV)	HDD of $nTiO_2$ (clay) (nm)	Hamaker Constant ($\times 10^{-20}$ J)	$\emptyset_{max}$ (k_BT)	$\emptyset_{2min}$ (k_BT)	ZP of $nTiO_2$ clay mixture (mV)	HDD of $nTiO_2$ clay mixture (nm)	A/A_0 (t=240 min)
5	$nTiO_2$	24.2±0.4	576±12	3.5	60.4	-0.3			1.01±0.01
	$nTiO_2$ + kaolinite	24.2±0.4 (-21.0±0.2)	576±12 (1135±10)	3.9	N/A	N/A	20.2±0.9	3966±405	1.15±0.01
	$nTiO_2$ + illite	24.2±0.4 (-30.2±0.6)	576±12 (506±10)	3.6	N/A	N/A	6.4±1.4	4664±1015	1.12±0.01
	$nTiO_2$ +montmorillonite	24.2±0.4 (-33.2±1.2)	576±12 (466±4)	3.3	N/A	N/A	-33.7±0.2	3049±14	1.13±0.01
9	$nTiO_2$	-28.1±1.0	522±8	3.5	72.0	-0.2			0.99±0.02
	$nTiO_2$ + kaolinite	-28.1±1.0 (-30.9±1.4)	522±8 (465±4)	3.9	83.9	-0.1	-19.4±0.0	888±7	1.06±0.03
	$nTiO_2$ + illite	-28.1±1.0 (-31.8±1.2)	522±8 (397±2)	3.6	78.8	-0.2	-24.2±0.8	493±18	1.03±0.02
	$nTiO_2$ +montmorillonite	-28.1±1.0 (-34.4±0.4)	522±8 (460±1)	3.3	93.4	-0.2	-32.7±3.5	514±5	1.03±0.03
5	$nTiO_2$+HA	-38.2±0.4	231±4	3.5	97.2	-0.2			1.01±0.01
	$nTiO_2$+kaolinite+HA	-38.2±0.4 (-21.0±0.2)	231±4 (1135±10)	3.9	69.5	-0.1	-36.5±0.4	238±2	1.01±0.00
	$nTiO_2$+illite+HA	-38.2±0.4 (-30.2±0.6)	231±4 (506±10)	3.6	92.1	-0.2	-36.9±0.3	237±6	1.01±0.01
	$nTiO_2$+montmorillonite+HA	-38.2±0.4 (-33.2±1.2)	231±4 (466±4)	3.3	102.3	-0.1	-37.2±0.3	233±4	1.01±0.01
9	$nTiO_2$+HA	-39.9±0.9	230±11	3.5	108.5	-0.2			1.00±0.01
	$nTiO_2$+kaolinite+HA	-39.9±0.9 (-30.9±1.4)	230±11 (465±4)	3.9	99.6	-0.2	-41.8±0.5	235±5	1.02±0.01
	$nTiO_2$+illite+HA	-39.9±0.9 (-31.8±1.2)	230±11 (397±2)	3.6	95.2	-0.2	-38.4±0.5	232±5	1.02±0.01
	$nTiO_2$+montmorillonite+HA	-39.9±0.9 (-34.4±0.4)	230±11 (460±1)	3.3	112.7	-0.1	-40.4±0.7	229±3	1.01±0.00

N/A: not applicable.

Table 6. The pH, Zeta Potential (ZP), and Hydrodynamic Diameter (HDD) of the suspensions in 0.1 mM $MgCl_2$ solutions, and the Energy Barrier ($\emptyset_{max}$) and Secondary Minimum ($\emptyset_{2min}$) calculated for the particle-particle interaction based on DLVO theory

pH	Suspension	ZP of $nTiO_2$ (clay) (mV)	HDD of $nTiO_2$ (clay) (nm)	Hamaker Constant ($\times 10^{-20}$ J)	$\emptyset_{max}$ (k_BT)	$\emptyset_{2min}$ (k_BT)	ZP of $nTiO_2$ clay mixture (mV)	HDD of $nTiO_2$ clay mixture (nm)	A/A_0 (t=240 min)
5	$nTiO_2$	36.1±0.2	624±4	3.5	160.4	-0.1			1.09±0.09
	$nTiO_2$+kaolinite	36.1±0.2 (-6.1±0.7)	624±4 (754±95)	3.9	N/A	N/A	11.9±1.2	295±3	1.06±0.05
	$nTiO_2$+illite	36.1±0.2 (-14.4±0.1)	624±4 (623±11)	3.6	N/A	N/A	25.9±0.2	3467±683	0.99±0.01
	$nTiO_2$+montmorillonite	36.1±0.2 (-30.9±0.6)	624±4 (256±3)	3.3	N/A	N/A	-17.8±1.0	5446±1254	1.02±0.01
9	$nTiO_2$	-9.4±0.4	5346±638	3.5	N/A	N/A			1.07±0.02
	$nTiO_2$+kaolinite	-9.4±0.4 (-19.7±0.5)	5346±638 (433±13)	3.9	19.1	-1.3	-8.9±0.5	7135±655	1.06±0.05
	$nTiO_2$+illite	-9.4±0.4 (-15.3±0.4)	5346±638 (396±8)	3.6	8.5	-1.5	-9.7±0.3	4844±72	1.07±0.07
	$nTiO_2$ +montmorillonite	-9.4±0.4 (-35.2±0.7)	5346±638 (261±3)	3.3	26.1	-0.6	-15.1±0.2	6003±1131	1.07±0.06
5	$nTiO_2$+HA	-18.7±0.3	235±1	3.5	32.2	-0.1			1.00±0.00
	$nTiO_2$+kaolinite+HA	-18.7±0.3 (-6.1±0.7)	235±1 (754±95)	3.9	8.0	-0.1	-14.2±1.2	301.7±2	1.00±0.00
	$nTiO_2$+illite+HA	-18.7±0.3 (-14.4±0.1)	235±1 (623±11)	3.6	26.1	-0.1	-16.0±0.6	254±1.4	1.00±0.00
	$nTiO_2$+montmorillonite+HA	-18.7±0.3 (-30.9±0.6)	235±1 (256±3)	3.3	57.4	-0.2	-19.3±0.1	317.3±3	0.99±0.01
9	$nTiO_2$+HA	-18.8±0.2	234±3	3.5	24.2	-0.2			1.00±0.00
	$nTiO_2$+kaolinite+HA	-18.8±0.2 (-19.7±0.5)	234±3 (433±13)	3.9	36.0	-0.1	-18.5±0.6	270.1±1	1.00±0.00
	$nTiO_2$+illite+HA	-18.8±0.2 (-15.3±0.4)	234±3 (396±8)	3.6	21.6	-0.1	-18.6±0.3	255.0±1	1.00±0.00
	$nTiO_2$+montmorillonite+HA	-18.8±0.2 (-35.2±0.7)	234±3 (261±3)	3.3	50.3	-0.1	-18.6±0.3	319.6±5	1.00±0.00

N/A: not applicable.

Table 7. The pH, Zeta Potential (ZP), and Hydrodynamic Diameter (HDD) of the suspensions in 1 mM $MgCl_2$ solutions, and the Energy Barrier ($\emptyset_{max}$) and Secondary Minimum ($\emptyset_{2min}$) calculated for the particle-particle interaction based on DLVO theory

pH	Suspension	ZP of $nTiO_2$ (clay) (mV)	HDD of $nTiO_2$ (clay) (nm)	Hamaker Constant ($\times 10^{-20}$ J)	$\emptyset_{max}$ (k_BT)	$\emptyset_{2min}$ (k_BT)	ZP of $nTiO_2$ clay mixture (mV)	HDD of $nTiO_2$ clay mixture (nm)	A/A_0 (t=240 min)
5	$nTiO_2$	37.1±0.1	301±5	3.5	120.4	-0.1			1.07±0.07
	$nTiO_2$+kaolinite	37.1±0.1 (-3.8±0.1)	301±5 (1759±151)	3.9	N/A	N/A	31.2±0.7	358±1	1.05±0.03
	$nTiO_2$+illite	37.1±0.1 (-14.0±0.2)	301±5 (1223±43)	3.6	N/A	N/A	25.4±0.1	4488±146	1.06±0.04
	$nTiO_2$+montmorillonite	37.1±0.1 (-16.4±0)	301±5 (1530±0)	3.3	N/A	N/A	-9.5±0.2	6322±983	1.01±0.02
9	$nTiO_2$	3.5±0.7	5426±549	3.5	N/A	N/A			1.15±0.01
	$nTiO_2$+kaolinite	3.5±0.7 (-2.0±0.2)	5426±549 (1422±212)	3.9	N/A	N/A	4.6±0.5	5493±648	1.02±0.00
	$nTiO_2$+illite	3.5±0.7 (-14.8±0.7)	5426±549 (1780±81)	3.6	N/A	N/A	12.2±0.2	4884±207	1.06±0.04
	$nTiO_2$ +montmorillonite	3.5±0.7 (-18.2±0.7)	5426±549 (1570±47)	3.3	N/A	N/A	-11.3±0.2	6726±170	1.02±0.00
5	$nTiO_2$+HA	-14.7±0.2	472±8	3.5	9.2	-0.4			1.16±0.01
	$nTiO_2$+kaolinite+HA	-14.7±0.2 (-3.8±0.1)	472±8 (1759±151)	3.9	19.0	-2.4	-11.7±0.7	944±17	1.12±0.03
	$nTiO_2$+illite+HA	-14.7±0.2 (-14.0±0.2)	472±8 (1223±43)	3.6	11.9	-2.5	-13.6±0.5	901±28	1.10±0.01
	$nTiO_2$+montmorillonite+HA	-14.7±0.2 (-16.4±0)	472±8 (1530±0)	3.3	17.3	-2.6	-15.0±0.7	1436±12	1.13±0.01
9	$nTiO_2$+HA	-15.4±0.2	1757±57	3.5	39.9	-3.2			1.13±0.01
	$nTiO_2$+kaolinite+HA	-15.4±0.2 (-2.0±0.2)	1757±57 (1422±212)	3.9	39.8	-3.0	-15.1±0.2	1966±74	1.17±0.01
	$nTiO_2$+illite+HA	-15.4±0.2 (-14.8±0.7)	1757±57 (1780±81)	3.6	34.1	-2.9	-14.9±0.3	1525±67	1.07±0.03
	$nTiO_2$+montmorillonite+HA	-15.4±0.2 (-18.2±0.7)	1757±57 (1570±47)	3.3	40.3	-3.5	-14.4±0.4	2211±124	1.16±0.03

N/A: not applicable.

Similar to that in 0.1 mM $MgCl_2$ solution, the HDD was very small (<360 nm) for the $nTiO_2$ and $nTiO_2$+kaolinite suspensions in 1 mM $MgCl_2$ solution at pH 5, indicating no aggregation. Stability of the $nTiO_2$ suspension was due to the high energy barrier between $nTiO_2$ particles (Table 7), as a result of the strong electrostatic charges of $nTiO_2$ (ZP = 37.1 mV) (Figure 5g). The small HDD of the $nTiO_2$+kaolinite suspension was inconsistent with the DLVO prediction (Table 7), and was likely caused by the hydrodynamic forces as discussed previously.

3.3.1.2. Effect of HA

HA was found to substantially hinder $nTiO_2$ aggregation. In the presence of 3 mg/L HA, no aggregation was observed, as evidenced by the small HDD (<320 nm) of the $nTiO_2$ and $nTiO_2$+clay suspensions under all the conditions in 3 mM NaCl and 0.1 mM $MgCl_2$ solutions (Figure 4c & 4f). In 1 mM $MgCl_2$ solution, the HDD of the $nTiO_2$ and $nTiO_2$+clay suspensions were relatively large (470−2200 nm) (Figure 4i). However, these HDD were comparable to those of the $nTiO_2$ and clay only suspensions in 1 mM $MgCl_2$ solution (Figure 4g), therefore the large HDD of the $nTiO_2$ and $nTiO_2$+clay suspensions was due to the large $nTiO_2$ and clay colloid size in 1 mM $MgCl_2$ solution, rather than aggregation.

HA stabilized the suspensions by adsorbing to $nTiO_2$ and changed the ZP of $nTiO_2$. At pH 5 in all the electrolyte solutions, and at pH 9 in 1 mM $MgCl_2$ solution, ZP of $nTiO_2$ changed from positive (Figure 5a, 5d, & 5g) to negative due to HA adsorption (Figure 5c, 5f, & 5i). At pH 9, ZP of the $nTiO_2$ became more negative in the presence of HA (Figure 5c, 5f, & 5i vs. Figure 5a, 5d,

& 5g). The change in ZP of the $nTiO_2$ in the presence of HA diminished the attractive forces between $nTiO_2$ particles, and the attractive forces between $nTiO_2$ and clay colloids, and therefore prevented aggregation. DLVO calculation showed that in the presence of HA, energy barriers existed between particles under all the conditions (Table 5, 6, and 7), indicating no aggregation, consistent with the observed small HDD. It was noted that in 1 mM $MgCl_2$ solution, secondary minima were present (-2.4 to -3.5 k_BT) (Table 7). However, aggregation was not observed under these conditions, presumably due to the hydrodynamic forces during shaking that acted against the secondary minima.

3.3.2. $nTiO_2$ deposition

In the presence of quartz sand, the absorbance (A/A_0) of the particle suspensions was either unchanged or substantially decreased during shaking (Figure 6). The absorbance of the same particle suspensions in the absence of the quartz sand, however, was either unchanged or slightly increased (Figure A4, Appendix 3). Therefore, the decrease of absorbance in systems with sand was attributable to $nTiO_2$ and/or $nTiO_2$–clay aggregates deposition to sand.

In 3 mM NaCl solution. In 3 mM NaCl solution at pH 5, the absorbance of the $nTiO_2$, $nTiO_2$+kaolinite, and $nTiO_2$+illite suspensions decreased to near zero within the first hour of mixing (Figure 6a), and the absorbance of the $nTiO_2$+montmorillonite suspension decreased to ~0.5 after 4 hours mixing. In all the experiments, the quartz sand carried negative charges (Figure

5b), however, the $nTiO_2$, $nTiO_2$+kaolinite, and $nTiO_2$+illite suspensions in 3 mM NaCl solution were all positively charged at pH 5 (Figure 5b), and therefore no energy barriers existed between these particles (i.e., $nTiO_2$ and $nTiO_2$+clay aggregates) and the quartz sand (Table 8), resulting in deposition and decrease in light absorbance (Figure 6a). For the $nTiO_2$+montmorillonite suspension, its ZP was negative (-34 mV) (Figure 5b), and DLVO calculation showed high energy barrier between $nTiO_2$+montmorillonite aggregate and the quartz sand, suggesting no deposition. The decrease of absorbance in this system was presumably due to direct $nTiO_2$ deposition onto the sand. When montmorillonite and quartz sand co-exist, they compete against each other for the positively charged $nTiO_2$, and some of the $nTiO_2$ may deposit onto the quartz sand without forming $nTiO_2$-montmorrillonite aggregates. For those $nTiO_2$ that formed $nTiO_2$-montmorrillonite aggregates, some may still attach to quartz sand via secondary minimum (-1.1 to -2.6 k_BT) (Table 8).

At pH 9, all the four suspensions were negatively charged (Figure 5b), and absorbance of the suspensions remained unchanged during mixing (Figure 6b), consistent with DLVO calculation results showing high energy barriers (>460 k_BT) and no secondary minima between particle and the quartz sand (Table 8).

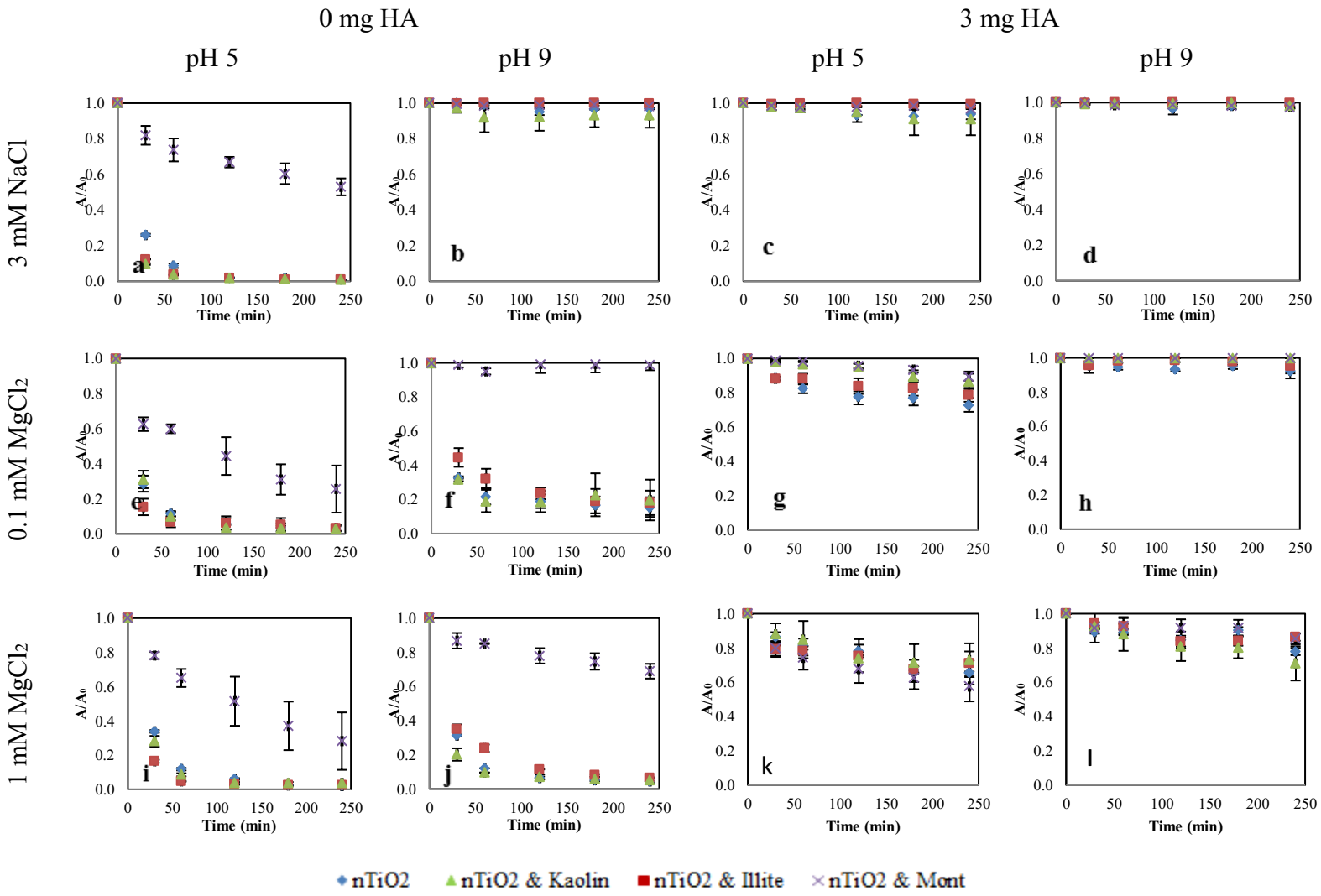

Figure 6. Relative absorbance (A/A_0) of the suspensions in the presence of quartz sand. Data is expressed as mean ± standard deviation of duplicate experiment

Table 8. The pH, Zeta Potential (ZP), and Hydrodynamic Diameter (HDD) of the suspensions in 3mM NaCl solutions, and the Energy Barrier ($\emptyset_{max}$) and Secondary Minimum ($\emptyset_{2min}$) calculated for the particle-sand interaction based on DLVO theory

pH	Suspension	ZP(mV)	HDD (nm)	Hamaker Constant ($\times 10^{-20}$ J)	$\emptyset_{max}$ (k_BT)	$\emptyset_{2min}$ (k_BT)	A/A_0 (t=240 min)
5	$nTiO_2$	24.2±0.4	576±12	1.4	N/A	N/A	0.01±0.00
	$nTiO_2$+kaolinite	20.2±0.9	3966±405	1.4 (0.55)	N/A	N/A	0..01±0.00
	$nTiO_2$+illite	6.4±1.4	4664±1015	1.4 (0.55)	N/A	N/A	0.01±0.00
	$nTiO_2$+montmorillonite	-33.7±0.2	3049±14	1.4 (0.55)	9498.0 (5680.1)	-2.6 (-1.1)	0.53±0.05
9	$nTiO_2$	-28.1±1.0	522±8	1.4	646.5	-0.5	0.97±0.00
	$nTiO_2$+kaolinite	-19.4±0.0	888±7	1.4 (0.55)	558.2 (626.2)	-1.0 (-0.3)	0.93±0.07
	$nTiO_2$+illite	-24.2±0.8	493±18	1.4 (0.55)	463.0 (524.7)	-0.5 (-0.2)	1.00±0.00
	$nTiO_2$ +montmorillonite	-32.7±3.5	514±5	1.4 (0.55)	812.3 (910.5)	-0.5 (-0.2)	0.98±0.02
5	$nTiO_2$+HA	-38.2±0.4	231±4	1.4	398.0	-0.2	0.94±0.03
	$nTiO_2$+kaolinite+HA	-36.5±0.4	238±2	1.4 (0.55)	387.1(449.5)	-0.2 (-0.1)	0.91±0.09
	$nTiO_2$+illite+HA	-36.9±0.3	237±6	1.4 (0.55)	390.1 (451.4)	-0.2 (-0.1)	0.99±0.01
	$nTiO_2$+montmorillonite+HA	-37.2±0.3	233±4	1.4 (0.55)	388.2 (449.9)	-0.2 (-0.1)	0.97±0.00
9	$nTiO_2$+HA	-39.9±0.9	230±11	1.4	488.2	-0.2	0.99±0.02
	$nTiO_2$+kaolinite+HA	-41.8±0.5	235±5	1.4 (0.55)	536.0 (610.1)	-0.2 (-0.1)	0.98±0.02
	$nTiO_2$+illite+HA	-38.4±0.5	232±5	1.4 (0.55)	463.6 (535.6)	-0.2 (-0.1)	1.00±0.00
	$nTiO_2$+montmorillonite+HA	-40.4±0.7	229±3	1.4 (0.55)	489.2 (568.2)	-0.2 (-0.1)	0.97±0.01

N/A: not applicable.

Table 9. The pH, Zeta Potential (ZP), and Hydrodynamic Diameter (HDD) of the suspensions in 0.1 mM $MgCl_2$ solutions, and the Energy Barrier ($\emptyset_{max}$) and Secondary Minimum ($\emptyset_{2min}$) calculated for the particle-sand interaction based on DLVO theory

pH	Suspension	ZP(mV)	HDD (nm)	Hamaker Constant ($\times 10^{-20}$ J)	$\emptyset_{max}$ (k_BT)	$\emptyset_{2min}$ (k_BT)	A/A_0 (t=240 min)
5	$nTiO_2$	36.1±0.2	624±4	1.4	N/A	N/A	0.03±0.02
	$nTiO_2$+kaolinite	11.9±1.2	295±3	1.4 (0.55)	N/A (N/A)	N/A (N/A)	0.03±0.01
	$nTiO_2$+illite	25.9±0.2	3467±683	1.4 (0.55)	N/A (N/A)	N/A (N/A)	0.03±0.02
	$nTiO_2$+montmorillonite	-17.8±1.0	5446±1254	1.4 (0.55)	1900.1 (2110.8)	-0.1 (-0.1)	0.26±0.13
9	$nTiO_2$	-9.4±0.4	5346±638	1.4	846	-0.1	0.15±0.06
	$nTiO_2$+kaolinite	-8.9±0.5	7135±655	1.4 (0.55)	1017.0 (1031.6)	-0.1 (-0.1)	0.19±0.12
	$nTiO_2$+illite	-9.7±0.3	4844±72	1.4 (0.55)	812.8 (889.0)	-0.1 (-0.1)	0.17±0.07
	$nTiO_2$ +montmorillonite	-15.1±0.2	6003±1131	1.4 (0.55)	1997.0 (2210.3)	-0.1 (-0.1)	0.94±0.03
5	$nTiO_2$+HA	-18.7±0.3	235±1	1.4	127.6	-0.1	0.73±0.04
	$nTiO_2$+kaolinite+HA	-14.2±1.2	301.7±2	1.4 (0.55)	104.4 (106.1)	-0.1 (-0.1)	0.87±0.04
	$nTiO_2$+illite+HA	-16.0±0.6	254±1.4	1.4 (0.55)	107.5 (108.1)	-0.1 (-0.1)	0.79±0.04
	$nTiO_2$+montmorillonite+HA	-19.3±0.1	317±3	1.4 (0.55)	112.1 (114.9)	-0.1 (-0.1)	0.90±0.03
9	$nTiO_2$+HA	-18.8±0.2	234±3	1.4	129.1	-0.1	0.93±0.07
	$nTiO_2$+kaolinite+HA	-18.5±0.6	270±1	1.4 (0.55)	145.3 (155.7)	-0.1 (-0.1)	1.00±0.00
	$nTiO_2$+illite+HA	-18.6±0.3	255±1	1.4 (0.55)	137.2 (148.9)	-0.1 (-0.1)	0.95±0.05
	$nTiO_2$+montmorillonite+HA	-18.6±0.3	320±5	1.4 (0.55)	172.2 (187.8)	-0.1 (-0.1)	1.00±0.00

N/A: not applicable.

Table 10. The pH, Zeta Potential (ZP), and Hydrodynamic Diameter (HDD) of the suspensions in 1 mM $MgCl_2$ solutions, and the Energy Barrier ($\emptyset_{max}$) and Secondary Minimum ($\emptyset_{2min}$) calculated for the particle-sand interaction based on DLVO theory

pH	Suspension	ZP(mV)	HDD (nm)	Hamaker Constant ($\times 10^{-20}$ J)	$\emptyset_{max}$ (k_BT)	$\emptyset_{2min}$ (k_BT)	A/A_0 (t=240 min)
5	$nTiO_2$	37.1±0.1	301±5	1.4	N/A	N/A	0.02±0.00
	$nTiO_2$+kaolinite	31.2±0.7	358±1	1.4 (0.55)	N/A (N/A)	N/A (N/A)	0.03±0.01
	$nTiO_2$+illite	25.4±0.1	4488±146	1.4 (0.55)	N/A (N/A)	N/A (N/A)	0.02±0.00
	$nTiO_2$+montmorillonite	-9.5±0.2	6322±983	1.4 (0.55)	630.1 (856.5)	-10.7 (-3.5)	0.26±0.17
9	$nTiO_2$	3.5±0.7	5426±549	1.4	N/A	N/A	0.04±0.00
	$nTiO_2$+kaolinite	4.6±0.5	5493±648	1.4 (0.55)	N/A (N/A)	N/A (N/A)	0.05±0.02
	$nTiO_2$+illite	12.2±0.2	4884±207	1.4 (0.55)	N/A (N/A)	N/A (N/A)	0.06±0.00
	$nTiO_2$ +montmorillonite	-11.3±0.2	6726±170	1.4 (0.55)	884.1 (1350.8)	-11.2 (-3.6)	0.63±0.04
5	$nTiO_2$+HA	-14.7±0.2	472±8	1.4	105.0	-0.7	0.66±0.07
	$nTiO_2$+kaolinite+HA	-11.7±0.7	944±17	1.4 (0.55)	135.9 (201.2)	-1.5 (-0.5)	0.73±0.09
	$nTiO_2$+illite+HA	-13.6±0.5	901±28	1.4 (0.55)	175.9 (238.2)	-1.4 (-0.5)	0.73±0.03
	$nTiO_2$+montmorillonite+HA	-15.0±0.7	1436±12	1.4 (0.55)	334.7 (449.6)	-2.1 (-0.7)	0.58±0.09
9	$nTiO_2$+HA	-15.4±0.2	1757±57	1.4	381.9	-2.7	0.74±0.02
	$nTiO_2$+kaolinite+HA	-15.1±0.2	1966±74	1.4 (0.55)	410.9 (565.5)	-3.0 (-1.0)	0.68±0.10
	$nTiO_2$+illite+HA	-14.9±0.3	1525±67	1.4 (0.55)	311.4 (438.7)	-2.4 (-0.7)	0.82±0.02
	$nTiO_2$+montmorillonite+HA	-14.4±0.4	2211±124	1.4 (0.55)	425.6 (590.7)	-3.4 (-1.1)	0.81±0.03

In the presence of 3 mg/L HA, at both pH 5 and 9, all the suspensions showed stable absorbance of $A/A_0 \approx 1.0$ during mixing (Figure 6c & 6d), indicating no deposition. ZP of the suspensions were all very negative (< -35 mV) (Figure 5c), attributable to HA adsorption to $nTiO_2$, consistent with previous reports (Tang and Cheng, 2018; Wu and Cheng, 2016). HA is well known for its ability to stabilize fine particles via electrostatic and steric effects (Aiken et al., 2011; Liu et al., 2011). DLVO calculations confirmed high energy barriers and no secondary minima between $nTiO_2$ (and $nTiO_2$-clay aggregates) and the quartz sand, due to the strong repulsive electrostatic forces (Table 8).

In 0.1 mM $MgCl_2$ solution. In the absence of HA, in 0.1 mM $MgCl_2$ solution at pH 5, the absorbance of the $nTiO_2$, $nTiO_2$+kaolinite, and $nTiO_2$+illite suspensions decreased to near zero in less than 150 minutes, and the absorbance of the $nTiO_2$+montmorillonite suspension reduced to 0.26 after 240 minutes (Figure 4e). The complete removal of $nTiO_2$ from water in the $nTiO_2$, $nTiO_2$+kaolinite, and $nTiO_2$+illite suspensions was due to the attractive electrostatic forces between $nTiO_2$ (and the $nTiO_2$+clay aggregates) and the quartz sand. At pH 5, all these three suspensions carried positive charges (Figure 5e), therefore no energy barriers existed and the particles were attracted to the quartz sand. In the $nTiO_2$+montmorillonite suspension, negatively charged quartz sand and montmorillonite competed against each other for the positively charged $nTiO_2$, and a fraction of the $nTiO_2$ were attracted to the sand via electrostatic attraction without

forming aggregates with montmorillonite. The $nTiO_2$-montmorillonite aggregates carried negative charges (ZP = -17.8 mV) (Figure 5e) and were repelled by the sand, hence the $nTiO_2$ in the aggregates remained in water. DLVO calculations confirmed high energy barrier and no secondary minimum between the $nTiO_2$-montmorillonite aggregate and the sand (Table 9).

At pH 9, the absorbance of the $nTiO_2$, $nTiO_2$+kaolinite, and $nTiO_2$+illite suspensions decreased to 0.15-0.19 after 240 minutes, indicating particle deposition. However, the absorbance of the $nTiO_2$+montmorillonite suspension remained unchanged ($A/A_0 \approx \sim 1.0$) throughout the experiment, indicating no deposition. ZP of all the four suspensions were negative at pH 9 (Figure 5e), and the DLVO calculation showed high energy barriers and no secondary minima (Table 9), suggesting no particle attachment to the sand. The DLVO results were consistent with the observations in the $nTiO_2$+montmorillonite suspension, but contradicted the results observed in the $nTiO_2$, $nTiO_2$+kaolinite, and $nTiO_2$+illite suspensions. Particle deposition in these three suspensions is likely caused by the bridging effect of Mg^{2+}, which connects negatively charged particles with the negatively charged sand surface. Due to the low affinity of quartz for Mg^{2+}, Mg^{2+} is unlikely to adsorb to quartz surface (Allen et al., 2017). The bridging effect is more likely caused by Mg^{2+} adsorption to Fe/Al oxyhydroxides, which have high affinity for cations at near neutral and alkaline pH (Fisher-Power et al., 2016; Mizutani et al., 2017). Both ICP-MS and SEM-EDX analyses confirmed the presence of Fe/Al oxyhydroxides in the sand. ICP-MS results indicated Fe

and Al concentration of 85 and 131 mg/kg respectively in the sand, and SEM-EDX results showed patch-wise Fe and Al oxyhydroxide coatings on sand surface (Figure A3, Appendix 2). The point of zero charge (PZC) of Fe and Al oxyhydroxides are usually around pH 7-8 (Tombácz, 2009). Therefore, Fe and Al oxyhydroxides presumably carried negative charges at pH 9 and strongly attract Mg^{2+}, which serves as a bridge between negatively charged particle and the Fe and Al oxyhydroxide coatings. In the $nTiO_2$+montmorillonite suspension, the bridging effect does not seem important, probably because of the much higher energy barrier (~2000 k_BT) between the particle and sand compared to that of other suspensions (~1000 k_BT) (Table 9).

In the presence of 3 mg/L HA, the absorbance of all the suspensions was high, e.g., the absorbance after 240 minutes was in the range of 0.73-0.90 at pH 5 and 0.93-1.00 at pH 9 (Figure 6g & 6h), indicating most of the particles remained suspended in water. DLVO calculation indicated high energy barriers and no secondary minima between particle and the sand, consistent with the experimental results. The low deposition was caused by HA adsorption to $nTiO_2$, which changed the ZP of $nTiO_2$ to negative at pH 5 (Figure 5f) and prevented $nTiO_2$ deposition. At pH 5, the removal of a small but substantial fraction of $nTiO_2$ (0.10-0.27) (Figure 6g) from water was likely due to the bridging effect of Mg^{2+}. $nTiO_2$ and Fe/Al oxyhydroxides are positively charged at pH 5 and have high affinity for HA (Wu and Cheng, 2016). Therefore, HA would adsorb to $nTiO_2$ and the Fe/Al oxyhydroxides on the sand, and Mg^{2+} could act as a “bridge” between HA

covered $nTiO_2$ and Fe/Al oxyhydroxides. At pH 9, $nTiO_2$ and Fe/Al oxyhydroxides are negatively charged, and their affinity for HA is low (Wu and Cheng, 2016). Therefore, HA adsorption should be low and the bridging effect was negligible.

In 1 mM $MgCl_2$ solution. At pH 5, in the absence of HA, the absorbance of all the suspensions substantially decreased during the experiments (Figure 6i), indicating a large fraction of the particles deposited. The deposition mechanisms were similar to those in 0.1 mM $MgCl_2$ solution, i.e., the attractive electrostatic forces between the positively charged particles and the negatively charged quartz sand (Figure 5h). For the $nTiO_2$+montmorillonite suspension, formation of negatively charged $nTiO_2$+montmorillonite aggregates (Figure 5h) helped to keep some $nTiO_2$ remain in water. It should be noted that at this high $MgCl_2$ concentration, a deep secondary minimum existed (-3.5~-10.7 k_BT, Table 10) and it may also contribute to $nTiO_2$ deposition.

At pH 9, absorbance of all the suspensions decreased in the 1 mM $MgCl_2$ solution (Figure 6j), indicating deposition. In the 0.1 mM $MgCl_2$ solution at pH 9, deposition was attributed to Mg^{2+} bridging. In the 1 mM $MgCl_2$ solution, however, ZP of the $nTiO_2$, $nTiO_2$+kaolinite, and $nTiO_2$+illite suspensions were all positive (Figure 5h), therefore energy barriers did not exist (Table 10) and deposition in these suspensions was caused by the attractive electrostatic forces between the particle and quartz surface. For the $nTiO_2$+montmorillonite suspension in 1 mM $MgCl_2$ solution, some $nTiO_2$ would deposit to the sand via attractive electrostatic forces instead of

forming $nTiO_2$-montmorillonite aggregates. Additionally, for the $nTiO_2$ that formed the negatively charged $nTiO_2$-montmorrillonite aggregates, they could deposit via a secondary minimum (-3.6 to -11.2 k_BT) (Table 10), and this may contribute to the lower absorbance in the 1 mM $mgCl_2$ (0.63) vs. that in 0.1 mM $MgCl_2$ solution (0.94).

Similar to its effect in the 0.1 mM $MgCl_2$ solution, HA in the 1 mM $MgCl_2$ solution substantially increased the absorbance at both pH 5 and 9 (Figure 6k and 6l vs. Figure 6i and 6j), indicating that HA reduced deposition. The lower deposition was caused by HA adsorption to $nTiO_2$, which changed the ZP of $nTiO_2$ to negative at pH 5 (Figure 5i) and prevented $nTiO_2$ deposition. Similar to the 0.1 mM $MgCl_2$ solution situation, DLVO calculation showed high energy barriers between particle and sand in the 1 mM $MgCl_2$ solution, which explains why most of the particles remained suspended. The mechanisms of particle deposition in the 1 mM $MgCl_2$ solution in the presence of HA were also similar to that in the 0.1 mM $MgCl_2$ solution, i.e., Mg^{2+} served as a bridge to connect the HA that adsorbed to $nTiO_2$ and Fe/Al oxyhydroxides. Compared to the 0.1 mM $MgCl_2$ solution, a larger fraction of particles deposited in 1 mM $MgCl_2$ solution (Figure 6k and 6l vs. Figure 6g and 6h). This could be attributable to the higher Mg^{2+} concentration and therefore, stronger bridging effect, and the secondary minima presented in the 1 mM $MgCl_2$ solution.

3.4. Summary

This study showed that $nTiO_2$ aggregation and deposition may occur simultaneously when negatively charged clay colloids compete against like-charged quartz sand for positively charged $nTiO_2$. Clay colloids and $nTiO_2$ formed hetero-aggregates (i.e., $nTiO_2$-clay aggregates) at pH 5 in 1 mM NaCl, 0.1 mM and 1 mM $MgCl_2$ solutions where $nTiO_2$ and clay colloid carried opposite charges. Clay colloids did not influence $nTiO_2$ aggregation at pH 9 in 3 mM NaCl and 0.1 mM $MgCl_2$ solutions due to the repulsive electrostatic forces between negatively charged $nTiO_2$ and clay colloids. In 1 mM $MgCl_2$ solution, however, $nTiO_2$ became positively charged at pH 9, and the negatively charged clay colloids promoted $nTiO_2$ aggregation by forming hetero-aggregates. The hetero-aggregates formed between $nTiO_2$ and clay may either deposit or remain suspended, depending on their interactions with quartz sand. In 3 mM NaCl and 0.1 mM $MgCl_2$ solution at pH 5, $nTiO_2$-kaolinite and $nTiO_2$-illite aggregates, along with $nTiO_2$, deposited onto quartz sand due to the electrostatic attraction. However, $nTiO_2$-montmorillonite aggregates remained in water due to electrostatic repulsion. At pH 9, in 3 mM NaCl solution, deposition did not occur due to electrostatic repulsion. However, in 0.1 mM and 1 mM $MgCl_2$ solution, deposition of $nTiO_2$ and/or $nTiO_2$+clay aggregates could be substantial due to Mg^{2+} bridging, electrostatic attraction, and secondary minimum. The presence of 3 mg/L HA was found to prevent $nTiO_2$ aggregation and deposition by changing the zeta potential of $nTiO_2$ in all the solutions at pH 5 and 9. In $MgCl_2$ solutions, however, HA can facilitate deposition via adsorbing to $nTiO_2$ and Fe/Al oxyhydroxides,

which enabled Mg^{2+} bridging. This study demonstrated that clay colloids may significantly affect $nTiO_2$ aggregation and deposition, and the effect of clay colloids is governed by the DLVO forces and Mg^{2+} bridging, which are influenced by pH, cation valance and concentration, co-existing HA, mineral type of the clay, and Fe/Al oxyhydroxide coatings on sand grains.

Acknowledgments

This work was supported by Natural Sciences and Engineering Research Council of Canada's Discovery Grant (402815-2012) and Canada Foundation for Innovation's Leaders Opportunity Fund (31836).

3.5. References

Aiken, G. R., Hsu-Kim, H., Ryan, J. N. 2011. Influence of dissolved organic matter on the environmental fate of metals, nanoparticles, and colloids. Environ. Sci. Technol. 45. 3196−3201.

Allen, N., Machesky, M. L., Wesolowski, D. J., Kabengi, N. 2017. Calorimetric study of alkali and alkaline-earth cation adsorption and exchange at the quartz-solution interface. Journal of Colloid and Interface Science 504. 538-548.

Bergström, L. Hamaker constants of inorganic materials. 1997. Advances in Colloid and Interface Science 70. 125–169.

Butt, H. J., Cappella, B., Kappl, M. 2005. Force measurements with the atomic force microscope: Technique, interpretation and applications. Surface Science Reports 59. 1-152.

Cai, L.; Tong, M.; Wang, X.; Kim, H. 2014. Influence of clay particles on the transport and retention of titanium dioxide nanoparticles in quartz sand. Environ. Sci. Technol. 48. 7323-7332.

Chen, G., Liu, X., Su, C. 2011. Transport and retention of TiO2 rutile nanoparticles in saturated porous media under low-ionic-strength conditions: measurements and mechanisms. Langmuir 27. 5393–5402.

Erhayem. M., Sohn, M. 2014. Stability studies for titanium dioxide nanoparticles upon adsorption of suwannee river humic and fulvic acids and natural organic matter. Science of the Total Environment 468-469. 249–257.

Feng, X., Simpson, A. J., & Simpson, M. J. 2005. Chemical and mineralogical controls on humic acid sorption to clay mineral surfaces. *Organic Geochemistry 36*(11). 1553-1566.

Fisher-Power, L. M., Cheng, T., Rastghalam, Z. S. 2016. Cu and Zn adsorption to a heterogeneous natural sediment: Influence of leached cations and natural organic matter. Chemosphere 144. 1973-1979.

Godinez, I. G., Darnault C. J. G. 2011. Aggregation and transport of nano-TiO_2 in saturated porous media: effects of pH, surfactants and flow velocity. Water Research 45. 839-851.

Gómez-Merino, A. I., Rubio-Hernández, F. J., Velázquez-Navarro, J.F., Galindo-Rosales, F.J., Fortes-Quesada, P. 2007. The Hamaker constant of anatase aqueous suspensions, Journal of Colloid and Interface Science 316. 451–456.

Gregory, J. 1981. Approximate expressions for retarded van der waals interaction. J. Colloid Interface Sci. 83. 138-145.

Han, P., Wang, X.T., Cai, L., Tong, M.P. and Kim, H. 2014 Transport and retention behaviors of titanium dioxide nanoparticles in iron oxide-coated quartz sand: Effects of pH, ionic

strength, and

humic acid. Colloids and Surfaces a-Physicochemical and Engineering Aspects 454. 119-127.

Hiemenz, P. C., Rajagopalan, R. 1997. Principles of colloid and surface chemistry, 3rd Ed. Marcel Dekker, Inc. New York.

Israelachvili, J. N. 2011. Intermolecular and surface forces (3rd ed). California, Academic Press.

Liu, X., Wazne, M., Chou, T., Xiao, R., Xu, S. 2011. Influence of Ca^{2+} and Suwannee River Humic Acid on aggregation of silicon nanoparticles in aqueous media. Water Research 45. 105-112.

Liu, X., Chen, G., & Su, C. 2012. Influence of collector surface composition and water chemistry on the deposition of cerium dioxide nanoparticles: QCM-D and column experiment approaches. Environmental science & technology 46(12). 6681-6688.

Loosli, F., Le Coustumer, P., Stoll, S. 2015. Effect of electrolyte valency, alginate concentration and pH on engineered TiO_2 nanoparticle stability in aqueous solution. Science of the Total Environment 535. 28-34.

Novich, B. E., Ring, T. A. 1984. Colloid stability of clays using photon correlation spectroscopy. Clays and Clay Minerals 32. 400-406.

Mizutani, K., Fisher-Power, L. M., Shi, Z., Cheng, T. 2017. Cu and Zn adsorption to a terrestrial sediment: Influence of solid-to-solution ratio. Chemosphere 175. 341-349.

Skocaj, M., Filipic, M., Petkovic, J., Novak, S. 2011. Titanium dioxide in our everyday life; is it safe? Radiology and Oncology 45. 227-247.

Solovitch, N., Labille, J., Rose, J., Chaurand, P., Borschneck, D., Wiesner, M. R., Bottero, J. 2010. Concurrent Aggregation and Deposition of TiO_2 Nanoparticles in a Sandy Porous Media. Environ. Sci. Technol. 44. 4897-4902.

Sposito, G., 1984. The Surface Chemistry of Soils. Oxford University Press, New York.

Tamura, H., Katayama, N., Furuichi, R. 1996. Modeling of Ion-Exchange Reactions on Metal Oxides with the Frumkin Isotherm. 1. Acid−Base and Charge Characteristics of MnO_2, TiO_2, Fe_3O_4, and Al_2O_3 Surfaces and Adsorption Affinity of Alkali Metal Ions. Science of The Total Environment 30. 1198-1204.

Tang, Z and Cheng, T. 2018. Stability and aggregation of nanoscale titanium dioxide particle ($nTiO_2$): Effect of cation valence, humic acid, and clay colloids. Chemosphere 192. 51-58.

Tombácz, E. 2009. pH-dependent surface charging of metal oxides. Periodica polytechnic 53. 77-86.

Van Olphen, H. 1963. An Introduction to Clay Colloid Chemistry. Interscience, New York.

Valera-Zaragoza. M., Yescas-Yescas. A., Juarez-Arellano. E.A., Aguirre-Cruz. A., Aparicio-Saguilán. A., Ramírez-Vargas. E., Sepúlveda-Guzmán. S., Sánchez-Valdes. S. (2014). Immobilization of TiO2 nanoparticles on montmorillonite clay and its effect on the morphology of natural rubber nanocomposites. Polymer Bulletin 71. 1295–1313.

Wainipee, W., Cuadros, J., Sephton, M. A., Unsworth, C., Gill, M. G., Strekopytov, S., Weiss, D. J. 2013. The effects of oil on As (V) adsorption on illite, kaolinite, montmorillonite and chlorite. Geochimica et Cosmochimica Acta 121. 487-502.

Wiesner, M.R. and Bottero, J.Y. 2007. Environmental Nanotechnology, The McGraw-Hill Companies, New York.

Wu, Y., Cheng, T. 2016. Stability of $nTiO_2$ particles and their attachment to sand: Effects of humic acid at different pH. Science of The Total Environment 541. 579-589.

Xu, N., Cheng, X., Zhou, K., Xu, X., Li, Z., Chen, J., Wang, D. and Li, D. 2017. Facilitated transport of titanium dioxide nanoparticles via hydrochars in the presence of ammonium in saturated sands: Effects of pH, ionic strength, and ionic composition. Science of the Total environment 612. 1348-1357.

Zhou, D., Abdel-Fattah, A. I., Keller, A. A. 2012. Clay Particles Destabilize Engineered Nanoparticles in Aqueous Environments. Environ. Sci. Technol. 46. 7520-7526.

Chapter 4. Conclusions

$nTiO_2$, one of the most extensively used nanoscale materials, have been universally utilized in products. $nTiO_2$ could easily be released into aquatic systems and cause environmental risks. Studying the fate of $nTiO_2$ in subsurface systems is essential for evaluating the environmental risks of $nTiO_2$. This thesis researched the influence of HA, clay colloids and water chemistry on $nTiO_2$ stability, aggregation and deposition onto quartz sand.

To ascertain the effect of cation valence, humic acid, and clay colloids on stability and aggregation of $nTiO_2$, batch experiments were conducted by mixing $nTiO_2$ with HA, or illite colloids or both in varying background solutions (Chapter 2). Results showed that in the absence of clay colloids and HA, ZP of $nTiO_2$ were generally more positive in $MgCl_2$ solutions than that in NaCl solutions at the same pH. When illite colloids and $nTiO_2$ particles co-existed, $nTiO_2$ were destabilized at $pH < pH_{pzc,TiO2}$ by illite colloids through formation of illite-$nTiO_2$ hetero-aggregates as a result of electrostatic attraction. At $pH > pH_{pzc,TiO2}$, illite colloids did not interfere with like-charged $nTiO_2$. Point of zero charge of $nTiO_2$ in $MgCl_2$ solution was higher than that in NaCl solution, and therefore hetero-aggregation in $MgCl_2$ solution occurred even at high pH. In both $MgCl_2$ and NaCl solutions, the presence of HA made $nTiO_2$ particles stable both in the absence and presence of illite colloids.

To ascertain how the presence of clay colloids, HA influence concurrent aggregation and deposition of $nTiO_2$ in varying background solutions, batch experiments were conducted by mixing $nTiO_2$, $nTiO_2$ & HA, $nTiO_2$ & clay colloids and $nTiO_2$ & HA & clay colloids with quartz sand in varying background solutions (Chapter 3). Results showed that $nTiO_2$ aggregation and deposition may occur simultaneously when negatively charged clay colloids compete against like-charged quartz sand for positively charged $nTiO_2$. The hetero-aggregates formed between $nTiO_2$ and clay may either deposit or remain suspended, depending on their interactions with quartz sand. In 3 mM NaCl and 0.1 mM $MgCl_2$ solution at pH 5, $nTiO_2$-kaolinite and $nTiO_2$-illite aggregates, along with $nTiO_2$, deposited onto quartz sand due to the electrostatic attraction. However, $nTiO_2$-montmorillonite aggregates remained in water due to electrostatic repulsion. At pH 9, in 3 mM NaCl solution, deposition did not occur due to electrostatic repulsion. However, in 0.1 mM and 1 mM $MgCl_2$ solution, deposition of $nTiO_2$ and/or $nTiO_2$+clay aggregates could be substantial due to Mg^{2+} bridging, electrostatic attraction, and secondary minimum. The presence of 3 mg/L HA was found to prevent $nTiO_2$ aggregation and deposition by changing the zeta potential of $nTiO_2$ in all the solutions at pH 5 and 9. In $MgCl_2$ solutions, however, HA can facilitate deposition via adsorbing to $nTiO_2$ and Fe/Al oxyhydroxides, which enabled Mg^{2+} bridging.

Appendix 1: Measuring light absorbance of the nTiO2 suspensions: wavelength selection

A UV-Vis spectrophotometer (Genesys 10S UV-Vis, Thermo Scientific) was used to measure light absorbance of the $nTiO_2$ suspensions. The UV-Vis spectra of $nTiO_2$ suspension (50 mg/L), and illite colloid suspension (10 mg/L illite) with 10 mg/L humic acid (HA) are shown in Figure A1. It is noted that absorbance of the $nTiO_2$ suspension is higher than that of the illite + HA mixture throughout the wavelength range of 200 to 800 nm. Additionally, at long wavelength, absorbance of the illite + HA mixture becomes negligibly low, but absorbance of the $nTiO_2$ suspension is still substantial. Based on this, a wavelength of 600 nm was chosen for measuring absorbance of the $nTiO_2$ suspensions to eliminate the influence of illite colloids and/or HA.

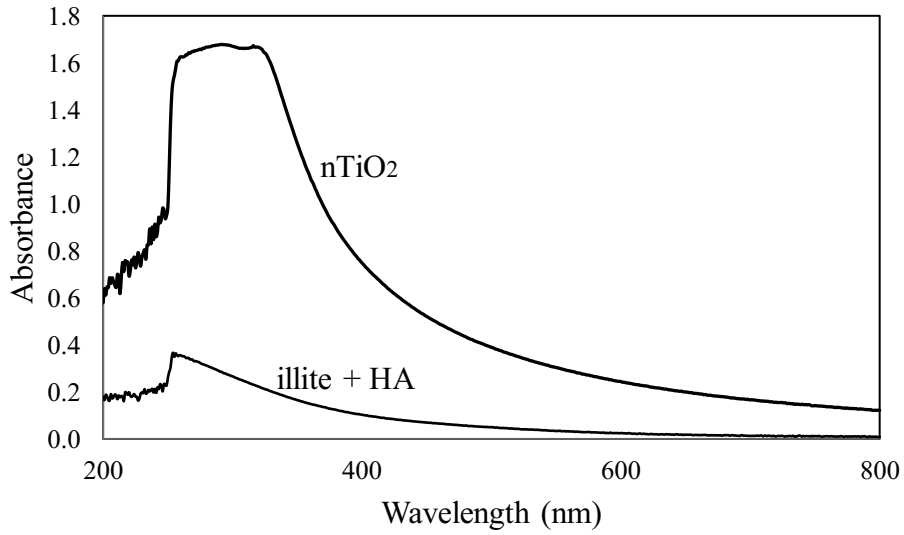

Figure A1. UV-Vis spectra of $nTiO_2$ suspension (50 mg/L), and illite + HA mixture (illite colloid = 10 mg/L, HA = 10 mg/L).

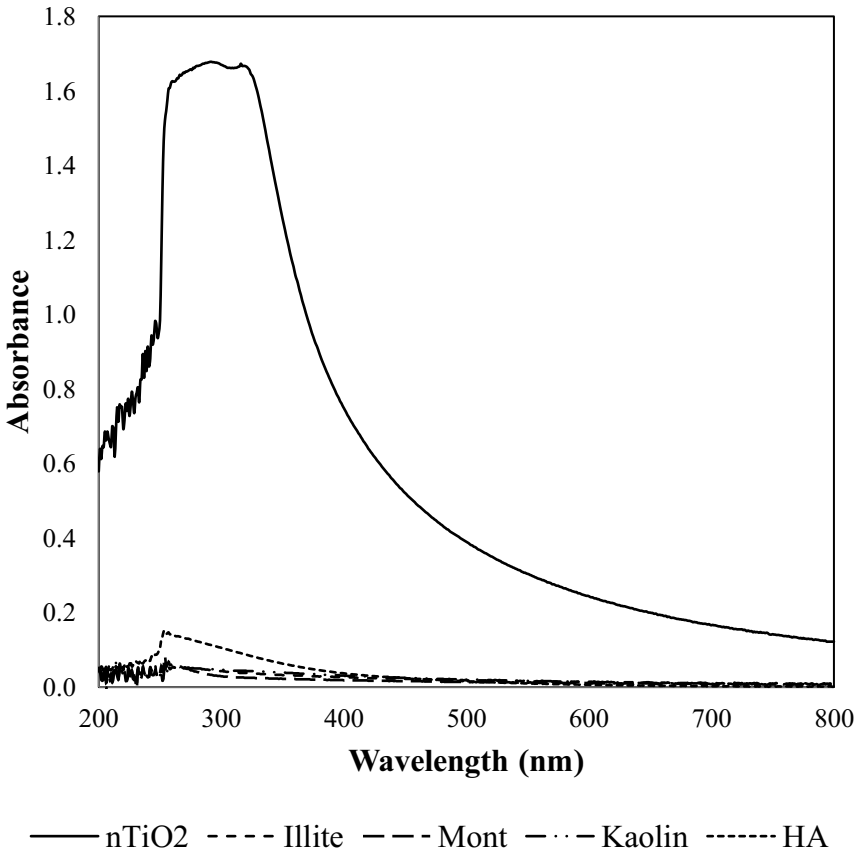

Figure A2. UV-Vis spectra of $nTiO_2$ (50 mg/L), illite (10 mg/L), montmorillonite (10mg/L), kaolinite (10 mg/L) and humic acid (HA) (3 mg/L) in deionized water.

Appendix 2: SEM-EDX results

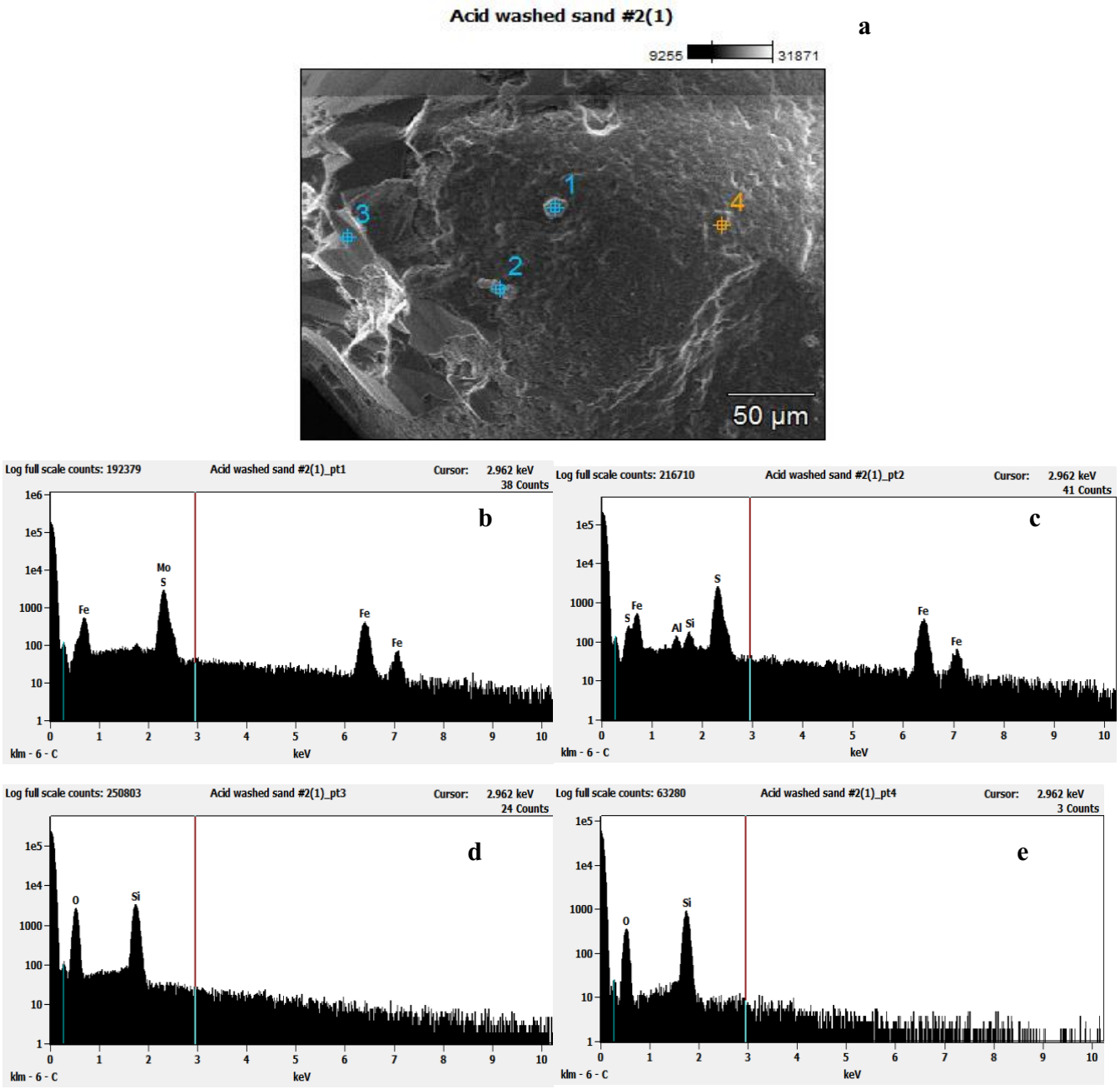

Fig. A3. SEM-EDX results of the quartz sand used in $nTiO_2$ deposition experiments.

*Four spots were checked by EDX. Spot 1 and 2 showed notable difference in surface features (panel (a)), and Fe and Al were detected by EDX (panel (b) and (c)). Spot 3 and 4 showed regular surface features (panel (a)), and only Si and O were detected by EDX (panel (d) and (e)).

Appendix 3: Shaking Stability

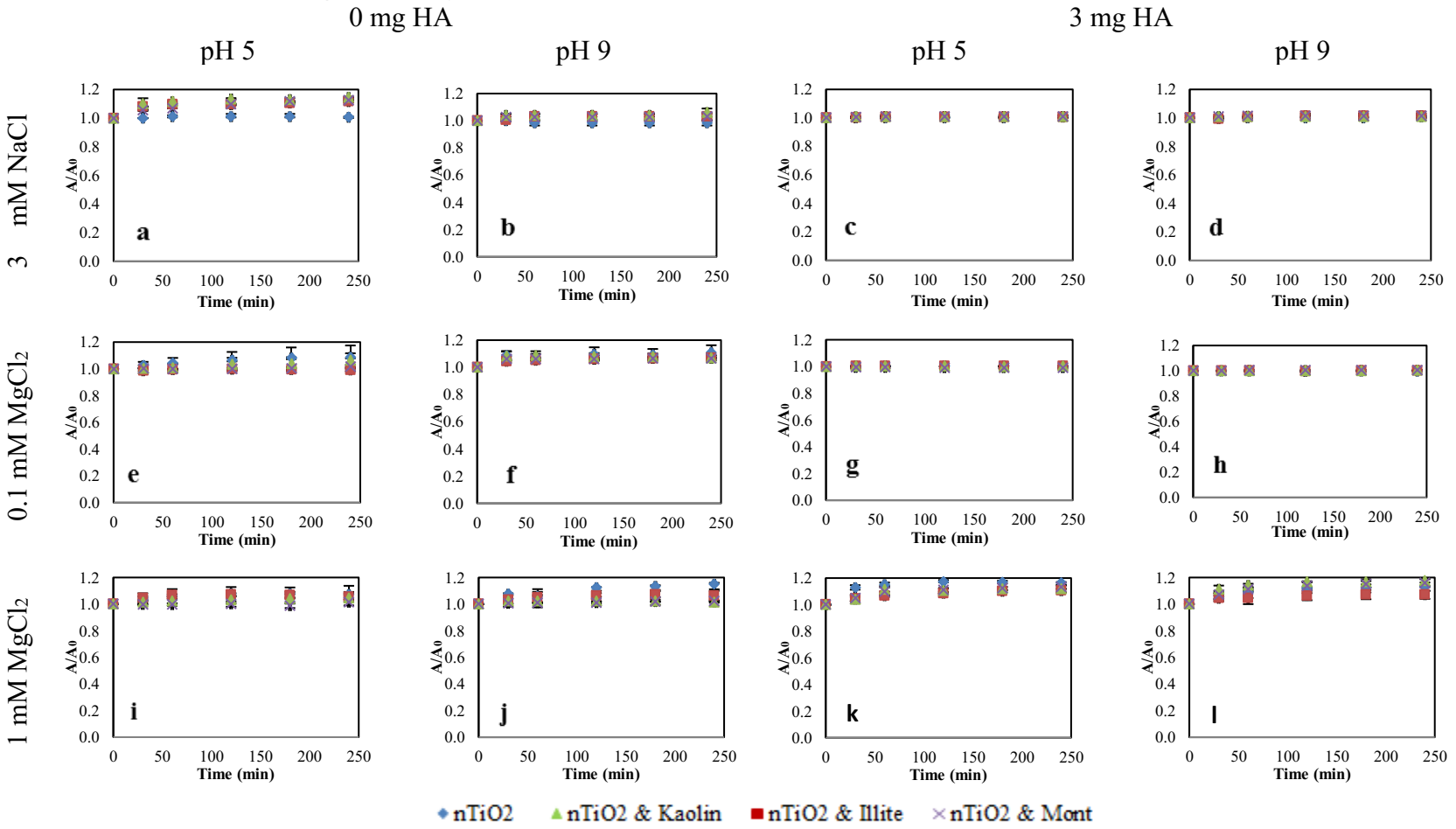

Figure A4. Relative absorbance (A/A_0) of the suspensions in the absence of quartz sand.